REVISION 2

Craters of the Moon National Monument Basalts as Unshocked Compositional and Weathering Analogs for Martian Rocks and Meteorites.

Christopher T. Adcock[1*], Arya Udry[1], Elisabeth M. Hausrath[1*], and Oliver Tschauner[1,2]

[1] Department of Geoscience, University of Nevada, Las Vegas (adcockc2@unlv.nevada.edu)

[2] High Pressure Science and Engineering Center, University of Nevada, Las Vegas

Short Title: Craters of the Moon National Monument Basalts and Mars

*Corresponding authors: Christopher T. Adcock (Christopher.Adcock@unlv.edu) and Elisabeth M. Hausrath (Elisabeth.Hausrath@unlv.edu)

Keywords

Mars, Analog, Craters of the Moon, Basalt, Martian Meteorite, Gusev Crater, Weathering, Age correlation

Abstract

The availability of terrestrial sites that are martian analogs allows researchers to investigate Mars using knowledge gained on Earth. Among the terrestrial analog sites for Mars is Craters of the Moon National Monument (COTM) in Idaho, USA. Craters of the Moon National Monument is home to over 60 basalt lava flows, many of which have been dated from 2,050 to 18,340 years before present (y.b.p.). Following previous authors, we examined the chemistry and petrogenesis of COTM basalts compared to basaltic martian rocks, martian meteorites, and meteorite clasts, and then examined the results of chemical weathering of the basaltic flows. Results of our comparative chemical analysis suggest COTM basalts are generally more evolved than the martian materials, with a few notable exceptions. Several COTM flow basalts, including rocks of the >18,000 year old Kimama flow, have high FeO, TiO_2, and P_2O_5 contents similar to the Wishstone and Watchtower class rocks analyzed at Gusev Crater, Mars, by the Mars Exploration Rover *Spirit*. The youngest basalts of COTM, such as those of the Minidoka (3890 y.b.p.) and Blue Dragon (2050 y.b.p.) flows have similarities in SiO_2, alkali contents, and mineralogical norms with select clasts in meteorite Northwest Africa – NWA – 7034. These similarities over a range of flow ages therefore suggest that COTM basalts have the potential to shed important light on specific igneous processes occurring on Mars.

Many of the basaltic rocks measured by rovers on Mars are thought to have experienced chemical weathering during aqueous interactions; however, few basalt weathering rates exist for

terrestrial Mars-relevant field environments to help interpret these processes. COTM, which has important similarities to some martian rocks discussed above, also represents a basalt flow chronosequence, and therefore allows for the investigation of basalt weathering as a function of time. We measured the depth of developed porosity in a suite of basalt flows ranging from 2,050 to 18,340 y.b.p., and compared field weathering relationships at COTM to weathering rinds developed on the Gusev Crater martian rocks Humphrey, Champagne, Mazatzal, and Wooly Patch. Our results indicate that depths of incipient weathering in COTM rocks increase with time at a rate of 2.32×10^{-2} to 3.04×10^{-2} $\mu m\ y^{-1}$, which is comparable to other terrestrial advance rates. Interestingly, this rate also indicates that chemical weathering strongly outpaces physical weathering even in this arid to semi arid environment. Weathering primarily of the matrix glass indicates that glass may be functioning as the profile-controlling mineral, which may have implications for chemical weathering in glass-rich rocks on Mars. Weathering rates of glass and other minerals can also help constrain the conditions (pH, temperature) of alteration on Mars. Of the altered martian rocks we compared to COTM (Humphrey, Champagne, Mazatzal, and Wooly Patch), altered surfaces of Mazatzal rock at Gusev Crater show the most similarities to weathered surfaces at COTM. Comparisons of chemical weathering in COTM basalts with altered surfaces of rocks in Gusev Crater, Mars, indicate Gusev Crater martian rocks have undergone significantly more aqueous alteration than that experienced by basaltic flows at COTM.

Introduction

Since the 1960's, dozens of robotic missions have been sent to Mars in an effort to better understand the planet (e.g. Steinbacher et al., 1972; Levinthal et al., 1973; Hess et al., 1976;

Snyder and Moroz, 1992; Golombek et al., 1997; Saunders et al., 2004; Zurek and Smrekar, 2007; Brückner et al., 2008; Smith et al., 2008; Soderblom and Bell III, 2008; Grotzinger et al., 2012). Data from these missions and martian meteorites (e.g. Bogard and Johnson, 1983) have greatly reshaped our views of the planet's interior and surface processes, potential martian habitability, and the possibility of life. Robotic missions and meteorite samples, however, have limitations, and many questions concerning martian interior and surface processes remain difficult to address. Rovers and landers have only explored a fraction of the martian surface and by necessity have analytical limitations. Orbiter and flyby missions collect regional and planet-wide data, but are limited to types of data which can be collected from orbit. Martian meteorites currently represent our only physical samples of Mars on Earth. However, these meteorites lack locational context, are not representative of the general martian crust, and have all been shocked in the processes that made them meteorites in the first place. This shock has altered their mineralogy and textures in ways that may not be obvious (Stöffler et al., 1986; Gooding, 1992; Rubin, 1992; Walton and Herd, 2007; McSween et al., 2009; McSween, 2015; Ody et al., 2015; Adcock et al., 2017). The availability of an unshocked analog to martian meteorites and rocks could yield numerous insights into both interior and surface processes on Mars.

One of the tools employed to advance our understanding of Mars has been the use of terrestrial martian analog sites. Planetary analogs can potentially fill gaps in our understanding or can supply reasonable assumptions where direct data are lacking. Martian analogs have allowed the investigation of Mars-relevant geomorphic, geochemical, petrogenetic, and hydrologic processes, as well as past or present potential habitability, by studying places on Earth (e.g. Breed, 1977; Wynn-Williams and Edwards, 2000; Greeley and Fagents, 2001; Arcone et al., 2002; Greeley et al., 2002; Wierzchos et al., 2006; Amils et al., 2007; Richardson et al., 2012).

Among the terrestrial analog sites for Mars is Craters of the Moon National Monument (COTM) (Peck, 1974; Greeley and King, 1977; Klingelhöfer et al., 2004; Weren et al., 2004; Brady et al., 2005; Heggy et al., 2006; McHenry, 2008; Usui et al., 2008; Richardson et al., 2012; Phillips-Lander et al., 2017), a 1600 km^2, arid to semi-arid basalt lava field located on the Snake River Plain of Idaho in the continental United States (Figure 1)(Kuntz et al., 1992). The area is the locale of 60, relatively high-phosphorus (up to 2.6 wt% P_2O_5), alkaline a'a' and pahoehoe basalt lava flows spanning eight eruptive periods and creating a volcanic chronosequence (Kuntz et al., 1986a; Vaughan, 2008; Vaughan et al., 2011). COTM lava flows generally consist of a glassy matrix with 0-30% olivine, 70-100% plagioclase, and minor abundances of pyroxenes (Putirka et al., 2009). A number of mineralogic, geologic, and landscape features at COTM, such as caves (Peck, 1974; Richardson et al., 2013; Phillips-Lander et al., 2017), the general basaltic terrain (Greeley and King, 1977; Heggy et al., 2006), igneous compositional and geomorphic analogs (Weren et al., 2004; Usui et al., 2008), or secondary minerals similar to some which may be on Mars (Peck, 1974; Klingelhöfer et al., 2004; Richardson et al., 2012), have made the region a useful martian analog in past studies (Peck, 1974; Greeley and King, 1977; Klingelhöfer et al., 2004; Weren et al., 2004; Brady et al., 2005; Heggy et al., 2006; McHenry, 2008; Usui et al., 2008; Richardson et al., 2012; Phillips-Lander et al., 2017).

In particular, Usui et al., (2008), suggested that the alkali basalts of COTM may be good analogs for the high phosphorus Wishstone and Watchtower class rocks at Gusev Crater, Mars. Usui et al., (2008), however, did not specify which specific COTM lavas might be good analogs. Many of the alkaline basalt flows at COTM possess elevated concentrations of FeO, TiO_2, and P_2O_5 (Stearns, 1928; Leeman et al., 1976; Kuntz et al., 1992; Stout et al., 1994) similar to Mars, which is generally elevated in FeO (2x higher than Earth) and P_2O_5 (10x higher than Earth) (Wanke and Dreibus, 1988; Taylor, 2013). Heterogeneous mantle sources, crustal contamination, or a combination of both have been proposed as possible explanations for the unusual chemistry at COTM (Kuntz et al., 1992; Stout et al., 1994; Reid, 1995; Usui et al., 2008), but the origins of the high-phosphorus basalts at COTM are not conclusively understood (Usui et al., 2008). Nevertheless, the high content in phosphorus and iron of some of the basalts at COTM suggests they are good compositional analogs for high-phosphorus rocks at Gusev Crater, Mars.

COTM basalts are also of interest to study surface processes such as chemical weathering. COTM represents an incipiently weathered basalt flow chronosequence with ages ranging between 2,050 and 18,340 y.b.p. (Vaughan, 2008) in an arid to semi-arid environment that, while wetter and warmer than present day Mars, may be analogous to a warmer and wetter martian environment of the distant past. Analysis of weathering processes occurring on these basalt flows may therefore shed light on the weathering processes that occurred on Mars. The Mars Exploration Rovers (MER) *Spirit* and *Opportunity* each carried an Alpha Particle X-ray Spectrometer (APXS) for elemental analyses (Rieder et al., 2003) and a Rock Abrasion Tool (RAT) for grinding into rocks to reach a "fresh" interior surface for analysis (Gorevan et al., 2003). APXS elemental analyses show changes in chemistry between the surface and interiors of rocks, an indication that chemical weathering and mineral dissolution may have occurred, developing weathering rinds by dissolution of the parent rocks (Klingelhöfer, 2004; Hurowitz et al., 2006a; Fleischer et al., 2008). The comparison between APXS analyses of outer rock surfaces and unaltered interiors allows constraints to be placed on chemical weathering and weathering rinds on the martian rocks. Previous analyses of weathered rocks at Gusev Crater have indicated dissolution of olivine and phosphate minerals, as well as potentially alteration of glass (Arvidson et al., 2004; Gellert et al., 2004; Hurowitz et al., 2006a; Squyres et al., 2006; Wang et al., 2006b; Hausrath et al., 2008b; Thomson et al., 2013; Adcock and Hausrath, 2015). Examination of weathering on the well-defined Craters of the Moon analog basalts may help shed light on the types of chemical weathering that have occurred on basaltic composition rocks on Mars.

In this study, therefore, we examine the composition of 26 COTM flow basalts and compare them to a range of martian meteorites, clasts within martian meteorites, and basaltic rocks analyzed on Mars. For comparisons, we use a sum of squares best-fit method, followed by elemental and calculated CIPW norm comparisons between rocks with good fits. We then select a set of COTM basalts spanning the full range of flow ages in the region (2,050 to 18,340 y.b.p) and investigate the relationship between the extent of aqueous weathering as indicated by changes in porosity and fracturing with depth over time to determine a field weathering relationship at COTM. COTM basalts are then compared to weathered rocks at Gusev Crater, Mars, to investigate aspects of chemical weathering on Mars.

Study Area Background

The COTM basalts are located in the northern part of the Great Rift volcanic zone and consist of lava flows, various cinder cones, and eruptive fissures (Kuntz et al., 1982). Russell (1903) is credited with the first general geologic studies of the COTM region during a regional geologic survey for the USGS spanning Cinder Butte, Idaho (southeastern Idaho) to Oregon along the Snake River Plain. Russell detailed much of the basaltic volcanism along the Snake River Plain, though the main objective of the study appeared to be documenting artesian aquifer, petroleum, and gas reservoirs. The first detailed geologic description specific to COTM was conducted in 1923 by Stearns (1924; 1928) for the Idaho Bureau of Mines and Geology. Stearns (1928) described the biota, geology, geomorphology, and reported the first chemical analysis of a COTM basalt, although it was not spatially located or assigned to a specific lava flow. Since those initial reports, the chemistry and mineralogy of many COTM flows have been well documented (Leeman et al., 1976; Kuntz et al., 1985; Kuntz et al., 1992; Stout et al., 1994) and a number of flows at COTM have been carbon-14 dated with calibrated ages ranging from 2,050 to >18,000 y.b.p. (Table 1, Supplementary Table S1)(Kuntz et al., 1986b; Kuntz et al., 1992; Vaughan et al., 2011).

Pedogenesis at COTM has also been previously documented, including as part of a Ph.D. dissertation (Vaughan, 2008; Vaughan and McDaniel, 2009; Vaughan et al., 2011). The succession of different ages of flows at COTM, and soil associated with them, represents a chronosequence. Vaughan (2008) observed that volcanic glass plays a significant role at COTM; flow basalts in the area generally contain 5-40% by volume glass within groundmass, although the glass content can exceed 65% by volume (Stout et al., 1994). Vaughan (2008) found that the proportion of weathered basaltic glass within soils associated with flows increases with the flow age.

COTM receives 240 to 380 mm Mean Annual Precipitation (MAP) moving from south to north (Stearns, 1928; Vaughan, 2008; Kukachka, 2010; Vaughan et al., 2011) making it an arid to semi-arid environment. The Mean Annual Temperature (MAT) for the region ranges from 6 to 9 °C depending on the specific location. Average monthly high temperatures range from -1.7 to 29 °C and average lows span -12 to 11 °C with sub-freezing lows prevailing much of the year (Kukachka, 2010).

The relatively fresh flows and volcanic structures at COTM led to the naming of the area and the choice of the region as a lunar surface analog to train astronauts during the Apollo era (Owen, 2008). Subsequent missions to the Moon and inner planets showed the COTM region to have features analogous to multiple planetary bodies, especially Mars (Greeley and King, 1977). The extensive, relatively barren, basalt flows, flow fields, shield volcanoes, and features such as lava tubes, caves, and channels, present a landscape that has increasingly been useful as an analog for Mars (Greeley and King, 1977; Weren et al., 2004; Brady et al., 2005; Heggy et al., 2006; McHenry, 2008; Phillips-Lander et al., 2017). In addition, the discovery of secondary sulfate minerals in COTM caves, including jarosite, which has also been found on Mars, suggests COTM caves may also be analogous to past martian environments (Peck, 1974; Klingelhöfer et al., 2004; McHenry, 2008; Farrand et al., 2009; Richardson et al., 2012; Cavanagh et al., 2015b; Phillips-Lander et al., 2017).

Methods

COTM and martian material selection and comparison approach

Chemical analyses of basalts from 26 different COTM flows spanning all eight eruptive periods at COTM were sourced from the literature (Supplementary Table S1) (Leeman et al., 1976; Kuntz et al., 1985; Kuntz et al., 1992; Stout et al., 1994). Selection criteria included basalts with good locational information, and associated age data. Similar to Kuntz et al. (1982) and to simplify data handling, we averaged lava composition analyses from the same eruptive ages or groups (from H – oldest - to A – youngest) for use in comparisons (Table 2). We also included

"C-low" and "A-low" groups, which were flows from the A and C eruptive ages with lower MgO content than other basalts from the same eruptive period.

For comparison to the chemical analyses of the COTM basalts described above, 28 representative martian meteorite bulk rock compositions were chosen spanning a range of martian meteorite types. These all display mafic to ultramafic composition, and include 5 poikilitic shergottites (gabbros and peridotites), 8 basaltic shergottites, 7 olivine-phyric shergottites (picritic basalts), 7 nakhlites (clinopyroxenites), 1 chassignite (dunite), and the orthopyroxenite Allan Hills (ALH) 84001 (Supplementary Table S2) (Lodders, 1998; Dreibus et al., 2000; Rubin et al., 2000; Barrat et al., 2002; Jambon et al., 2002; Shirai and Ebihara, 2004; Gillet et al., 2005; Day et al., 2006; Ikeda et al., 2006; Anand et al., 2008; Lin et al., 2008; Treiman and Irving, 2008; Basu Sarbadhikari et al., 2009; McSween et al., 2009). The meteorites vary in age from 4.0 Ga to 165 Ma and originate from different localities on Mars. All of these meteorites fall within the basalt envelope in the Total Alkali-Silica (TAS) diagram (Figure 2). We note that nakhlites, chassignites, and poikilitic shergottites are mafic and ultramafic cumulates rather than basalts and as such would not normally appear on a TAS diagram. However, because these meteorites are considered in comparisons within this study, we have included them in Figure 2, similar to some previous studies (e.g. McSween et al., 2009; McSween, 2015). We also include 17 clasts from within meteorite Northwest Africa (NWA) 7034 (Santos et al., 2015) (Supplementary Table S3). Unlike the other meteorites, which all display an evident igneous texture, NWA 7034 is a polymict breccia that consists of basaltic, trachy-andesitic, Fe-, Ti-, P-rich (FTP) clasts, as well as impact melt clasts (Udry et al., 2014; Santos et al., 2015). These different clasts likely originate from different sources and were formed by different igneous and impact processes (Santos et al., 2015). The bulk rock composition of NWA 7034 was therefore not considered in this study, because, as a polymict breccia, it does not represent a true igneous rock.

In addition to martian meteorites, COTM chemical compositions were also compared to igneous compositions measured by *Spirit* (n = 93) using the APXS instrument at Gusev Crater (Supplementary Table S4) from sols 14 to 470 of the mission (Brückner et al., 2008). We also included Bounce Rock major element compositions measured by the *Opportunity* rover in Meridiani Planum; this surface rock is unique as it is the only rock analyzed on Mars that shows a shergottitic composition (Zipfel et al., 2011). Although not a meteorite, we included Bounce Rock in the appended martian meteorite table based on its shergottitic composition and connection with martian meteorites (Supplementary Table S2) (Zipfel et al., 2011). Dust on the surface of martian rocks is known to influence APXS analyses (e.g. Arvidson et al., 2006; Berger et al., 2016) and many of the rocks at Gusev Crater have also undergone chemical weathering and have altered surfaces as discussed above (Arvidson et al., 2006; Hurowitz et al., 2006a; Hurowitz et al., 2006b; McSween et al., 2006; Squyres et al., 2006; Hurowitz and McLennan, 2007; Hausrath et al., 2008b; Adcock and Hausrath, 2015). Therefore, the chemical composition comparison with COTM focuses on the 11 rocks that were RAT-abraded, and thus have available analyses with the lowest degree of alteration or dust contamination (Supplementary Table S5) (Squyres et al., 2006; Brückner et al., 2008). These RAT-treated rocks comprised seven rock classes identified at Gusev Crater as the Adirondack, Clovis, Wishstone, Watchtower, Backstay, and Independence classes (Squyres et al., 2006; Brückner et al., 2008).

Finally, we compared the COTM lavas to the fine-grained alkaline rocks (n=3) measured by the *Curiosity* rover ChemCam instrument in the early Hesperian-aged Gale Crater (Sautter et al., 2015) (Supplementary Table S6). These rocks are unique among martian surface rocks as they are both enriched in SiO_2 and alkalis. We chose the fine grained "Group 2" class described as aphyric effusive volcanic rocks as they are texturally more similar to COTM lavas (Putirka et al., 2009; Sautter et al., 2015).

To quantitatively compare COTM lava compositions to martian igneous compositions from martian meteorites and measurements from Gusev Crater, Meridiani Planum, and Gale Crater, we used a sum of squares best-fit method, where differences between the mean COTM basalt major element compositions (i in Eq. 1 below, where i = SiO_2, TiO_2, Al_2O_3, FeO_T, MnO, MgO, CaO, Na_2O, K_2O, and P_2O_5) for a given eruptive period (x), and analytical values from martian igneous rocks (x') are squared and summed (after Wheater and Cook, 2006):

$$\text{best fit index} = \sum_i (x_i - x'_i)^2 \qquad \text{[Eq. 1]}$$

We obtained a best-fit index for each composition comparison, where a low index represents similar compositions and a high index indicates different compositions (Supplementary Tables S2 to S6). We then calculated and compared the normative mineralogies for martian and COTM compositions with low indices indicating similar compositions using the CIPW norm (Supplementary Table S7).

Analysis of weathering through time of high-phosphorus COTM basalts

Materials and sample preparation. To investigate weathering over time at COTM, six of the 23 compiled COTM basalt flows were selected and sampled based on previous chemical characterizations (Kuntz et al., 1992), location confidence, the presence of associated available carbon-14 ages (Kuntz et al., 1992), elevated P_2O_5 concentrations (based on the generally higher phosphorus concentrations measured on Mars), and with an effort to span the entire eruptive age range at COTM (Table 1, Supplementary Table S1). Exposed surface lava flow samples were collected in order to maximize the probability of collecting in place samples that had been exposed to weathering for the entire age of the flow. Locations of the sample sites covered a geographically wide region of COTM to minimize any local climate effects (Figure 1). Published carbon-14 age data were calibrated using Calib 7.0.4 with InterCal 13 (Table 1) (Stuiver and Reimer, 1993).

From the six collected samples, representative pieces of basalt were removed and oriented in epoxy mounts so that subsequent thin sectioning would produce sections, which included exposed/weathered surfaces as well as a cross-section into the rock perpendicular to the weathered surface. Thin sections were then made with a 0.3 μm final polish using anhydrous cutting and polishing methods. Epoxy impregnation was also used in an effort to preserve weathered material and soluble minerals during sample preparation.

Sample and image analyses. Scanning Electron Microscopy (SEM) analyses were performed on prepared thin sections using a JEOL JSM 5600 (EMiL Facility, University of Nevada Las Vegas) at 20 kV, a 30-40 spot size setting, and a working distance of 20 mm in both Backscattered Electron (BSE) and Secondary Electron Imaging (SEI) modes. The spot size setting on the JEOL JSM 5600 is a unitless, relative scale. Analysis of acquired images indicated spot size remained below 200nm and the estimated theoretical minimum beam diameter was 30-45nm (based on Goldstein et al., 1992). Analysis focused on characterizing the texture of the rocks, as well as image collection and measurement of any development of apparent alteration rinds and weathering-induced porosity or fracturing. Energy Dispersive Spectroscopy (EDS) analyses were carried out using an Oxford Instruments detector and Oxford INCA software with semi-quantitative capabilities to analyze qualitative mineral major element compositions, when needed to confirm general mineralogy and phases of interest.

Subsequent off-line image analysis was performed using *Adobe Photoshop CS6* software. Thicknesses of apparent weathering rinds were measured and relative changes in porosity and fracturing with depth were investigated using backscattered electron (BSE) image mosaics. To construct the mosaics, overlapping images (typically 7) were collected at 250x magnification from the weathered surface of the samples into unweathered core material to a depth of at least 1200 μm into the sample (well into interior parent material that showed no surface effects). Location selection was generally random within representative weathered areas with the exception that the area was first inspected to ensure the mosaic would not intersect large cracks, fractures, or vesicles. Mosaics were then manually assembled in *Adobe Photoshop CS6* to avoid any distortions added by automation software. Plots of porosity with depth were constructed from the mosaics by first aligning, rotating, and cropping the mosaic images such that 10 μm thick "slices" of equal areas of the sample image parallel to the weathered sample surface could be consecutively isolated, contrast enhanced, and processed to determine the amount of open micro-porosity as an area % value (example Supplementary Figure S1). This high contrast porosity mapping method is similar to methods previously used to measure porosity development with weathering in basalts (Gordon and Brady, 2002). The resulting values were recorded and then plotted against depth (Supplementary Figure S2 and Table S8). Macro-pores (>100 μm on a side) were excluded to avoid counting large vesicles as developed porosity. The surface porosity was considered to be the average of the top 100 μm of the sample. The average porosity of the interior was based on the deepest 100 μm of the sample (1100 μm to 1200 μm interval).

Results

Terrestrial and martian composition comparisons

The different COTM rock compositions vary from tephrite to trachyte (Figure 2, Table 2, Supplementary Table S1) and eruptive group chemistries range between 45.2-61.4 wt% SiO_2, 0.4-4.5 wt% MgO, 3.3-8.1 wt% CaO, 12.9-14.9 wt% Al_2O_3, 16.3-19.2 wt.% FeO, and 0.2-2.6 wt% P_2O_5. The different eruptive periods become more evolved with time, corresponding to an increase in SiO_2, alkalis (Na_2O+K_2O), Al_2O_3, and FeO, and a decrease in CaO and P_2O_5 (Figures 2 and 3). The major element compositions of COTM eruptive groups therefore show alkaline evolutionary trends (Figure 2). The different lavas contain 50-55% normative plagioclase, 13-22% normative orthoclase, 0-18% normative hypersthene, and 0-15% normative olivine. The lava groups C, C-low, and A-low are also quartz-normative. In contrast to COTM rock compositions, most of the martian igneous compositions are located in the basaltic field in the TAS diagram (Figure 2). Despite this difference, some compositional comparisons between rocks of specific COTM eruptive periods and martian igneous materials produce good best-fits (Table 3).

As observed in our best-fit calculations and elemental diagrams, martian meteorites and COTM compositions differ significantly in major element chemistry (Figures 2 and 3, Supplementary Table S2). Martian meteorites are generally enriched in MgO and FeO and depleted in Al_2O_3 and alkalis compared to COTM rocks (Figures 2 and 3). The basaltic shergottite compositions yield the closest fits when compared to COTM basalts, mainly with older COTM flows of eruptive periods F and E. However, like the other martian meteorites, these meteorites also show lower alkali, higher FeO_T and MgO contents, and generally different major element chemistries fropm the COTM rocks (Figures 2 and 3, Supplementary Table S2).

The clasts within NWA 7034 are in general, like most martian materials, alkali poor compared to COTM rocks (Figure 2). NWA 7034 clasts are also generally MgO rich and Al_2O_3 poor compared to COTM materials (Figure 3). However, a number of the NWA 7034 clasts (e.g. clasts 6, 56, 66, 70 and 74F) show a closer fit to COTM lavas than the other martian meteorites (Figures 2 and 3; Supplementary Table S3). Normative mineralogies of these clasts are the most similar to COTM lavas A and B, although they contain higher normative hypersthene (Supplementary Table S7). Clasts 77, 31, FTP 15, and FTP 64 have somewhat poorer fits than those discussed above, but do have SiO_2 and MgO contents comparable to some COTM basalts (Supplementary Table S3). Clast FTP 15 is also similar in Al_2O_3, FeO, and CaO to COTM basalts, though very high in P_2O_5 relative to COTM rocks (8.65 wt% versus 2.64 wt%).

COTM basalts differ significantly in chemical composition when compared to the Gusev igneous rocks except for the RAT-treated Gusev Crater rocks Champagne and Wishstone (both Wishstone class rocks) and Watchtower. This result is illustrated in the TAS diagram as well as other comparison plots where Wishstone class rocks fall within the groupings of COTM basalts (Figures 2 and 3). The best-fit calculations and normative mineralogies of COTM lavas of episode H are overall most similar to these Gusev Crater rocks (Supplementary Tables S4, S5 and S7). However, FeO in the Gusev rocks is generally slightly lower (12.2 wt.%, n=3, versus 15.1 wt.%, n=23 in COTM lavas) and P_2O_5 is higher in Wishstone class rocks (5.1 wt%, n=3 vs. 2.64 wt.% in COTM lavas) (Figures 3A and 3B, Supplementary Table S5).

The alkaline "Group 2" rocks at Gale Crater are generally different from the COTM flows in major element composition due to their evolved nature and high SiO_2 and Na_2O content (Supplementary Table S6). However, despite higher alkali and Al_2O_3, in the Group 2 rocks, both major element compositions and normative mineralogies (especially in Group 2 rock Becraft) are similar to COTM A-low and C-low lavas (Supplementary Tables S6 and S7).

Weathering of high-phosphorus COTM basalts

Observations of thin sections by SEM BSE imaging revealed textures that are generally vitrophyric and aphanitic (Figure 4). The grain size and texture of the matrix material varies between the different basalts, with samples from flows Minidoka and Blue Dragon possessing a glassy matrix (Figure 4A and B), and samples from Lava Point, Prong Horn, Sunset, and Kimama exhibiting a lower proportion of glass in the groundmass (Figure 4C through E). Silica-rich surface coatings, some showing laminations (e.g. Figure 4C and D, Figure 5), were observed on exposed surfaces of all samples. The coatings were up to 100 μm thick. These features are similar to coatings previously observed in Antarctica, northern Scandinavia, Svalbard, Karkevagge, and cooler semi-arid regions of Hawaii (e.g. the Ka'ū desert), and are thought to result from water-rock interactions in relatively cold and arid or semi-arid environments (Farr and Adams, 1984; Curtiss et al., 1985; Dixon et al., 2002; Hausrath et al., 2008c; Salvatore et al., 2013). The coatings were not continuous over significant distances and sharp breaks in the coatings suggested that in many places they had been removed by spalling (e.g. Figure 5).

The Blue Dragon sample, from the youngest of the flows sampled, displayed dark layers (in BSE imagery) in some places that were distinctly different from the coatings. These layers were ~10 μm thick, always into glassy matrix, and always at or near the exposed surface of the samples (Figure 6). The chemistry of the dark layers as measured by EDS compared to the glass did not appear significantly different.

Measurements of porosity from exposed surfaces into the interiors of the samples indicated that increases in fractures and porosity occur to greater depths than the thickness of the coatings (which were up to 100 μm thick) (Figure 5). Surfaces of older rocks showed generally greater depths of porosity than younger rock surfaces (Supplementary Figure S1). Average porosities of exposed surface material ranged from 0.58 - 7.5% with an overall average porosity of 3.8%. The porosity of interior material varied from 0.08 % to 0.98 % with an average value of 0.6%. While these values may seem low, the technique used here does not measure macroporosity and the values are within the range of porosities of basalts measured by others (Freeze and Cherry, 1977; Sato et al., 1997; Rejeki et al., 2005).

Discussion

COTM lavas as analogs for martian igneous rocks.

The relative rarity and shock history of all martian meteorites make the potential availability of unshocked terrestrial analogs significant. Such analogs to a martian meteorite or rock could yield numerous insights into both martian interior and surface processes. In addition, the analogs could shed light on the implications of shock on martian meteorites, or meteorites in general. There are, however, overall crucial differences between COTM lavas and martian meteorite compositions, notably the alkali enrichments and lower MgO content of COTM lavas

This is a preprint, the final version is subject to change, of the American Mineralogist (MSA)
Cite as Authors (Year) Title. American Mineralogist, in press.
DOI: http://dx.doi.org/10.2138/am-2018-6193

(Figures 2 and 3). COTM lavas also have generally higher P_2O_5 and TiO_2 contents than martian meteorites. In addition, the mineralogies and textures (mostly plagioclase and olivine phenocrysts in a microcrystalline to glassy/vitrophyric matrix) observed in the COTM lavas have not been observed in martian meteorites (McSween, 2015). These differences are almost certainly due to the evolved nature of the COTM parent magmas. COTM lava compositional trends observed in Figures 2 and 3 represent fractional crystallization and assimilation of the crust (intermediate to felsic composition) by the parental magma, which likely originated from the upper mantle/lower crust (Kuntz et al., 1992; Putirka et al., 2009). However, the martian crust is mostly basaltic (McSween et al., 2009), and thus, assimilation of the crust on Mars would not generally result in such evolved lava compositions.

One potential exception to the contrasts of martian meteorite materials and COTM basalts are clasts within NWA 7034. A number of NWA 7034 clast compositions and normative mineralogies are closer to the COTM lavas than the martian meteorites (Figure 2). Most notably, clasts 56 and 74F show elevated alkali contents compared to most martian igneous compositions and are compositionally close to younger lavas at COTM (Supplementary Table S3). Clasts in NWA 7034 (and paired meteorites) are from a variety of sources and COTM basalts make good analogs on a case by case basis.

The alkaline rocks of Gale Crater show geochemical similarities to the most evolved COTM lavas. However, the rocks may not be petrogenetically similar. The high-SiO_2 and alkali signatures of Gale Crater rocks are likely due to extensive fractional crystallization for the martian rocks (Gazel and McSween, 2016) rather than crustal assimilation as is the case for the COTM rocks (Kuntz et al., 1992).

In contrast to the alkaline rocks of Gale Crater, COTM bulk-rock chemistries compared to RAT-treated APXS rock analyses at Gusev Crater indicate that most of these martian rocks come from much less evolved parent sources than the COTM rocks. Wishstone class rocks at Gusev Crater, however, show a good compositional fit with COTM lavas (Figures 2 and 3). These results are consistent with Usui et al. (2008), who suggested COTM rocks were potential analogs to Wishstone class rocks. Usui et al. (2008) did not specify a particular flow or eruptive period as the best analog for Wishstone class rocks, and analyses from multiple eruptive periods are good matches with the Wishstone rock class (Figures 2 and 3, Supplementary Table S5). Sum of squares calculations from analytical comparisons in this study indicate rocks of eruptive period H may be the closest in composition to martian Wishstone class rocks, suggesting Kimama basalt flow rocks as good chemical analogs (Supplementary Table S5). These lavas are among the oldest and least evolved at COTM and enriched in FeO and P_2O_5 compared to the other eruptive periods. Specific flows from other eruptive periods are also close in chemistry, including Pronghorn (eruptive period F) and Lava Point basalts (eruptive period E). The high-Mg group basalts of eruptive period C are additional good matches with Wishstone class rocks. The similarities between COTM and Wishstone class rocks are due to the elevated FeO, TiO_2, and P_2O_5 contents, above what is typical in terrestrial and martian basalts, respectively. While Mars rocks in general are elevated in FeO and P_2O_5 compared to terrestrial basalts (Taylor, 2013), Wishstone class rocks are even more so, and the enrichments in P_2O_5 in COTM and Wishstone-class rocks are both likely due to metasomatization of their mantle source by CO_2-rich fluids and the formation of xenocrystic phosphate minerals. This suggests a potential common history between the rocks (Ming et al., 2006; Usui et al., 2008).

Caution, nevertheless, should generally be applied when considering terrestrial analogs like COTM basalts. Wishstone class rocks, for instance, are often discussed as basaltic igneous rocks, tephrites, or mafic rocks, which have been metasomatized (McSween et al., 2006; Ming et al., 2006; e.g. Usui et al., 2008; Adcock and Hausrath, 2015). Consistent with this interpretation, CIPW norms have been used to investigate Wishstone class rocks by several authors (e.g. McSween et al., 2006; Ming et al., 2006; Ruff et al., 2006; McSween et al., 2008; Usui et al., 2008). However, angular textures in RAT abraded surfaces and the lighter color tone of Wishstone class rocks have also been interpreted as pyroclastic, and thus the rocks may be tuffs (Arvidson et al., 2006; Ming et al., 2006; Squyres et al., 2006). Further, their occurrence as only float rocks or as clasts in a geologic sub-units suggests they are impact excavated rocks from a deeper stratigraphic unit at Gusev Crater (Crumpler et al., 2011). Therefore they are potentially shock altered or even impact derived (Squyres et al., 2006). Without additional data, petrogenesis of these martian rocks is difficult to constrain. The fact that both rock types have likely experienced similar metasomatization, are igneous in origin, and have chemical similarities, however, suggests that the COTM rocks are useful analogs for Wishstone class rocks in applications where an exact petrogenetic match is not required.

Weathering of COTM basalts and implications for rock weathering at Gusev Crater, Mars

In order to examine the effect of weathering with time in the basaltic chronosequence present at COTM, we compared the weathering present at exposed surfaces of samples of six COTM flows of different ages. Coatings were observed on the surfaces of each of the samples (e.g. Figures 4C, 4D, and 5). These silica-rich coatings were up to 100 μm thick and consistent with coatings seen on other terrestrial basalts (Farr and Adams, 1984; Curtiss et al., 1985; Dixon et al., 2002; Hausrath et al., 2008c; Salvatore et al., 2013). Boundaries between coatings and underlying surfaces were sharp. The origin of the coatings is thought to be tied to weathering processes and aqueous interactions, with the most commonly proposed formation mechanisms involving mineral dissolution and subsequent precipitation of the coatings onto the rock surface (Farr and Adams, 1984; Curtiss et al., 1985; Dixon et al., 2002; Hausrath et al., 2008c; Salvatore et al., 2013). This type of mechanism could explain the layered appearance and why the coatings do not seem influenced by underlying material. The exact source of the chemistry for coatings is not conclusively known and likely variable (Farr and Adams, 1984; Salvatore et al., 2013). In some cases the source of the chemistry of the coatings is thought to be the rock itself (e.g. Dixon et al., 2002), and in other cases the source is proposed to be external, such as from eolian deposition or solution transport (Farr and Adams, 1984; Curtiss et al., 1985). Such coatings are susceptible to spalling (Farr and Adams, 1984; Curtiss et al., 1985), and those on COTM samples were no exception; no correlation between age and thickness could be confirmed likely due to spalling off of the rock coatings.

The Blue Dragon sample, from the youngest of the flows sampled (Blue Dragon) known for its blue sheen, also possessed rock coatings like the other samples. However, it additionally displayed dark layers (in BSE imagery) in some places that were different than the coatings (Figure 6). These layers were only observed in contact with glassy matrix and at or near exposed surfaces, suggesting they are weathering related. However, they are chemically indistinguishable from the underlying glass by EDS. This, along with the lower backscatter signal observed in BSE imagery, may indicate they are of a lower density than the underlying glass material and may be the product of hydration (e.g. Bindeman and Lowenstern, 2016). Blue Dragon is the only sample where these dark layers were observed.

Rock weathering generally results in the loss of the most rapidly dissolving or soluble minerals in the rock first (Goldich, 1938). Examination of weathered surfaces at COTM indicate that dissolution of glass resulting in increased porosity has occurred (Figure 5), but little alteration of crystalline materials is observed, including apatite or olivine. This dissolution of glass is consistent with observations by Vaughan (2008) who noted mainly glass weathering at COTM. This is also a similar scenario to previous results in arid environments, including those of Hausrath et al. (2008b; 2008c) who observed dissolution of glass matrix surrounding crystalline material (including olivine) within the rocks at Svalbard, Norway. Therefore, we interpreted enhanced porosity as resulting from glass dissolution due to chemical weathering, and measured changes in porosity with depth as a function of age of the lava flow, which was assumed to correlate with duration of exposure to weathering conditions.

The depth of weathering-enhanced porosity within samples was interpreted in three ways (Figure 7). First, BSE image mosaics that had been contrast enhanced to reveal porosity (see methods) were visually examined, and the apparent depth of enhanced porosity was judged by the viewer visually (Supplementary Figure S3). Similarly, the apparent depth of enhanced porosity was estimated visually from plotted profiles of porosity measured as described above in the methods (Supplementary Figure S1). Finally, the apparent depth of enhanced porosity was estimated as occurring when three consecutive 10 μm slices gave measured porosities of less than the average porosity documented from the 700 μm to 1200 μm interval of the BSE mosaic (i.e. the porosity of the unweathered material) plus the standard deviation of the porosity measurements. The second of the three consecutive values was then selected as the depth of

This is a preprint, the final version is subject to change, of the American Mineralogist (MSA)
Cite as Authors (Year) Title. American Mineralogist, in press.
DOI: http://dx.doi.org/10.2138/am-2018-6193

weathering-induced porosity (Supplementary Table S8). Because the first two techniques are subject to visual interpretation, they were carried out four times by the same individual (Supplementary Table S9). We used an average of all four observations, which also allowed us to calculate a standard deviation for the repeated observations.

We then examined the relationship between lava flow age and depth of weathering-induced porosity in COTM material by plotting porosity depth observations for each thin section/sample against age and then analyzing by linear regression. Linear regression trends were forced through zero (i.e. no depth = no duration of weathering). Standard deviations (or other error) of observations were not given weight in the regression. Calculations were performed in *OriginPro 2017* software.

Linear regression fits of depth of developed porosity versus time in COTM rocks produced R^2 values indicating a correlation of depth of developed porosity with age (Figure 7). The two visual approaches of determining the depth of weathering-induced porosity had exceptionally high R^2 values (0.88 and 0.86) (Figure 7C & D). This could be, in part, an effect of biasing by the observer since the same person made all of the determinations. However, although the R^2 value from the interpretation using numerical values for internal porosity is lower (0.59), it groups well with, and produces a similar slope to, the other interpretations. While the different techniques used to interpret depth of weathering porosity produced slightly different results (Figure 7), they all showed the same general correlation between depth of developed porosity and age (Figure 7A). Regression slopes were all similar and produced advance rates between 2.32×10^{-2} and 3.04×10^{-2} µm y^{-1} (Figure 7 B-D).

These findings indicate that, even in an arid environment such as Craters of the Moon, chemical weathering outpaces physical weathering. Previous examinations of arid environments

DOI: http://dx.doi.org/10.2138/am-2018-6193

have indicated the strong importance of physical erosion. Typical erosion rates for basaltic rocks in arid environments on Earth range from 1×10^{-1} to 3×10^{1} μm y^{-1} (Greeley et al., 1984; Nishiizumi et al., 1986; Nishiizumi et al., 1991; Bierman, 1994;). However, a broad range of factors control physical erosion rates, making them highly variable (Sharp, 1964; Sharp, 1980; Greeley and Iversen, 1987; Millot et al., 2002). Sharp (1964), for instance, observed almost no physical weathering of crystalline rocks in over a decade of observation at Coachella Valley, California, one of the most vigorous eolian abrasion environments known (Greeley and Iversen, 1987). That study determined limited abrasive supply in the location to be the cause - a situation possible at COTM. Thus, the exact physical weathering contribution occurring at COTM is difficult to constrain.

The presence of surface coatings on samples and the correlation between age and depth of developed porosity suggests erosional weathering rates are low at COTM. Discontinuous coatings and sharp breaks in coatings suggest spalling off of these coatings. However, in contrast to Hausrath et al. (2008b), who proposed significant spalling of enhanced porosity due to glass dissolution in their rocks from Svalbard, we see no evidence of similar effects at COTM. Spalling at COTM appears limited to thin surface coatings. This may be due to the freeze-thaw process being important in arctic arid environments such as Svalbard (Yesavage et al., 2015). Steady state between chemical and physical erosion has often been assumed (Brantley and White, 2009). Results here showing increasing depth of developed porosity with time, crucially, indicate that such a steady state has not yet been developed after 18,000 years at COTM.

Weathering advance rates determined by linear regression analysis Figure 7) produced rates of glass dissolution into the surface of our rocks of between 2.32×10^{-2} and 3.04×10^{-2} μm y^{-1}. Comparing our COTM weathering advance rates to weathering advance rates of matrix glass dissolution in other arid environments, Hausrath et al., (2008b) estimated glass dissolution depths in basalts at Svalbard as 250 μm, which, assuming a deglaciation of <80,000 years ago (Landvik et al., 1998; Yesavage et al., 2015) and noting the repeated spalling, would indicate a weathering advance rate of > 3 x 10^{-3} μm y^{-1}. This is consistent with our measured COTM weathering advance rate of between 2.32 x 10^{-2} and 3.04 x 10^{-2} μm y^{-1}.

Comparing our COTM weathering advance rate to basalt chemical weathering advance rates in general, Navarre-Sitchler and Brantley (2007) compiled overall weathering advance rates for basalts based on rind thickness from several studies (Porter, 1975; Colman and Pierce, 1981; Oguchi and Matsukura, 1999; Sak et al., 2004). In that study, basalt weathering advance rates ranged from 6.0 x 10^{-3} to 2.8 x 10^{-1} μm y^{-1}. Thus advance rates determined here are within the range of previous studies for basalts in general.

Another crucial observation is the very small amount of porosity generated by glass dissolution in COTM rocks, and the fact that no dissolution of other phases was observed (Supplementary Table S8 and Figure S1). This suggests that the glass in these rocks is functioning as the profile-controlling mineral – the first mineral to dissolve and thus generate porosity allowing water transport and therefore dissolution of other minerals (Brantley and White, 2009). The presence of a profile-controlling mineral has been inferred from deep profiles (Jin et al., 2010), but is difficult to observe at this resolution except during very incipient weathering such as that occurring at COTM. This observation that glass is the profile-controlling mineral in COTM, similar to glass dissolution in Svalbard (Hausrath et al., 2008), also suggests that glass dissolution may be important in incipient weathering on Mars.

Evidence for the possible presence of glass has been found at multiple locations on Mars (Christensen et al., 2004; McSween et al., 2008; Bish et al., 2013; Cavanagh et al., 2015). XRD refinements of soils at Rocknest, Gale Crater, for instance, suggest an amorphous component of ~27 to 45 wt. % best fit by basaltic glass and/or allophane (or similar) and potentially minor amounts of metal-sulfides or sulfates (Bish et al., 2013; Blake et al., 2013; Dehouck et al., 2014). Similar amounts were found in Confidence Hills, a sedimentary rock outcrop at Gale Crater (Cavanagh et al., 2015). At Meridiani Planum, the Mini-Thermal Emission Spectrometer (MiniTES) on *Opportunity* indicated glass in a number of rock outcrops (Christensen et al., 2004). The MiniTES on *Spirit* at Gusev Crater also indicated potentially significant glass components in rocks such as Barnhill class (McSween et al., 2008).

Dissolution rates of glass versus other rapidly dissolving minerals such as olivine and phosphate-bearing minerals have been previously used to infer both temperature and pH (Hausrath et al., 2008a; Hausrath et al., 2008b; Adcock and Hausrath, 2010; Hausrath and Tschauner, 2013; Yen et al., 2016). In this case, temperatures at COTM are relatively low (MAT 6° - 9° C) and the region experiences sub-freezing lows for a significant part of the year (Kukachka, 2010). Vaughan (2008) measured soil pH at COTM and determined values of 3.4 - 5.7, which are extremely acidic soil pHs for an arid soil formed on basaltic parent material. At these pH conditions, olivine dissolution would be faster than dissolution of a basaltic glass. However, these were soil pH values associated with COTM flows and the study noted vegetation had a strong control on pH. The COTM samples examined in this study were not buried in soil, but exposed, and thus not influenced heavily by vegetation. Under these conditions, pH during aqueous interactions would likely be higher than those measured at COTM. Hausrath (2008c) measured pH values of 8.5 and 6.75 in unvegetated weathering basaltic areas in Svalbard. At the low temperatures present at COTM, glass dissolution would be favored over olivine dissolution at pH values of ~7.5 or higher (Hausrath et al., 2008c; Schieber et al., 2016). At 25°C glass dissolution is favored over apatite at a pH of ~6 or higher and the crossover pH decreases somewhat with decreasing temperature (Gislason and Oelkers, 2003; Palandri and Kharaka, 2004; Wolff-Boenisch et al., 2004; Bandstra et al., 2008; Hausrath et al., 2008c; Adcock et al., 2013).

Weathered surfaces that may be similar to those observed at COTM have been previously studied at Gusev Crater using various approaches. The Specific Grind Energy (SGE) of RAT operations has been used as an indicator of relative weathering between rocks at Gusev Crater (Arvidson et al., 2004; Myrick et al., 2004; Squyres et al., 2006; Wang et al., 2006a; Herkenhoff et al., 2008; Thomson et al., 2013). Schroeder et al. (2006) used Mössbauer spectrometery to study alteration in the surfaces of Gusev Crater rocks based on which Fe phases were present. Selective depth Mössbauer using two gamma energies has also been applied to examine thickness of weathering rinds in Gusev rocks (Fleischer et al., 2008). The data that are most comparable to our observations of COTM, and on which we focus, are changes in chemistry with depth from the altered surface of the rock to the less altered RAT-abraded surface (Arvidson et al., 2006).

Changes in chemistry with depth in these RAT abraded Gusev Crater rocks suggest the development of a weathering profile, and have been used to interpret the dissolving minerals, pH, and duration of martian alteration (Hurowitz et al., 2006a; Ming et al., 2006; Wang et al., 2006b; Hurowitz and McLennan, 2007; Hausrath et al., 2008b; Ming et al., 2008; Adcock and Hausrath, 2015). For example, Mg and Fe depletion on the surface of Humphrey (Supplementary Table S10) has been used as an indicator of olivine dissolution under acidic conditions (Hurowitz et al., 2006a; Hurowitz and McLennan, 2007; Hausrath et al., 2008b) and used to constrain the duration of alteration (Hausrath et al., 2008b). Calcium and P depletions from the surface of

Watchtower and Wishstone have been inferred to result from either acidic (Hurowitz et al., 2006b; Ming et al., 2006) or near-neutral dissolution (Adcock and Hausrath, 2015) of a phosphate mineral or minerals (Supplementary Table S10). Wooly Patch is a moderately altered igneous outcrop of basaltic chemical composition, although SGE values suggest it is likely a competent tuff rather than basalt (Wang et al., 2006b; Ming et al., 2008). Glass dissolution may have occurred in the Wooly Patch outcrop of Gusev Crater, based on Al and Si depletions at the surface and evidence of phyllosilicates associated with the outcrop (Supplementary Table S10) (Wang et al., 2006b). This potential glass dissolution or alteration has been inferred to have occurred in a mildly (pH 4–6) acidic environment (Wang et al., 2006b). .

Of the RAT treated rocks at Gusev Crater, Mazatzal (Adirondack class) weathering may be the most similar to weathering occurring at COTM. Mazatzal is thought to contain both glass and olivine (e.g. Hamilton and Ruff, 2012), and depletions of Ca and Al at the surface of Mazatzal relative to the interior (Supplementary Table S10) suggest glass may have been dissolving from this rock, and depletions in Mg and Fe suggest dissolution of olivine (Hurowitz and McLennan, 2007). Dissolution of both olivine and glass at near-freezing temperatures would indicate either near-neutral or highly acidic conditions (Hausrath et al., 2008b; Schieber et al., 2016).

Mazatzal also has a complex rock coating and evidence of salts in vugs and veins of the rock suggesting it was weathered, at least at some point, under brine conditions (Haskin et al., 2005). Brines have been shown to inhibit the dissolution of a range of minerals to a similar extent with decreasing activity of water (Pritchett et al., 2012; Dixon et al., 2015; Olsen et al., 2015; Steiner et al., 2016), and thus increase the duration of time necessary to achieve a given weathering depth. Therefore the multiple mm scale depth of the apparent weathering in Mazatzal could suggest a history with a significantly long period of aqueous interactions compared to COTM.

Implications

With the exception of the Moon, the exploration of other bodies in our solar system has been restricted to remote observations or robotic missions. The only physical samples of these other bodies (if any) are meteorites, which are both rare and have undergone shock metamorphism. Terrestrial planetary analogs, like Craters of the Moon National Monument, offer a way to study chemical, physical, and environmental aspects of other planets, such as Mars, in the absence of direct human visitation or sampling.

Though COTM lavas flows are generally more evolved than martian materials, an examination of COTM flow chemistries in this study indicates COTM rocks from select eruptive periods are potentially good compositional analogs based on chemistry and normative mineralogy of specific rocks on Mars, martian meteorites, or clasts within martian meteorites (Table 3). Among the best compositional comparisons are Wishstone class martian rocks found at Gusev Crater with older basalts of COTM, most specifically, rocks of the ~18,000 year old Kimama lava flow (eruptive period H). Clast 6 within NWA 7034 also shows some compositional similarities with Kimama lava flow rocks.

Weathering in the basaltic flows at COTM is also informative regarding martian weathering. The predominantly glass dissolution occurring at COTM sheds light on potential glass dissolution in multiple rocks on Mars, particularly the enhanced glass dissolution at very low pH and near-neutral pH conditions at Gusev Crater. The observed correlation of depth of incipient weathering with flow age at COTM, even after ~18,000 years, is unexpected and indicates the dominance of chemical weathering over physical weathering at COTM. It also suggests relatively long weathering times for altered rocks at Gusev Crater, Mars, furthering our understanding of the martian environment.

Acknowledgements

This research is funded through NASA grants NNX10AN23H and NNX15AL54G. Additional funding was provided by a Nevada Space Grant Consortium fellowship, a GSA research grant to C. Adcock, and a UNLV GPSA travel grant. The authors thank A. Simon, E. Smith, H. Sun, P. Forster, V. Tu, S. Gainey, and M. Steiner for assistance related to this work, as well as the National Park Service for permission to sample at Craters of the Moon National Monument. We would also like to thank Jeff Taylor, Tomohiro Usui, and Javier Cuadros for their valuable input during the review and editing process.

References

Adcock, C.T., and Hausrath, E.M. (2010) Kinetic Studies of Phosphate Containing Minerals and Implications for Mars. 42nd Lunar and Planetary Conference, p. 2177. Lunar and Planetary Institute, Houston, TX.

---. (2015) Weathering Profiles in Phosphorus-Rich Rocks at Gusev Crater, Mars, Suggest Dissolution of Phosphate Minerals into Potentially Habitable Near-Neutral Waters. Astrobiology, 15(12), 1060-1075.

Adcock, C.T., Hausrath, E.M., and Forster, P.M. (2013) Readily available phosphate from minerals in early aqueous environments on Mars. Nature Geoscience, 6(10), 824-827.

Adcock, C.T., Tschauner, O., Hausrath, E.M., Udry, A., Luo, S.N., Cai, Y., Ren, M., Lanzirotti, A., Newville, M., Kunz, M., and Lin, C. (2017) Shock-transformation of whitlockite to merrillite and the implications for meteoritic phosphate. Nature Communications, 8, 14667.

Amils, R., González-Toril, E., Fernández-Remolar, D., Gómez, F., Aguilera, Á., Rodríguez, N., Malki, M., García-Moyano, A., Fairén, A.G., and de la Fuente, V. (2007) Extreme

This is a preprint, the final version is subject to change, of the American Mineralogist (MSA)
Cite as Authors (Year) Title. American Mineralogist, in press.
DOI: http://dx.doi.org/10.2138/am-2018-6193

environments as Mars terrestrial analogs: the Rio Tinto case. Planetary and Space Science, 55(3), 370-381.

Anand, M., James, S., Greenwood, R., Johnson, D., Franchi, I., and Grady, M. (2008) Mineralogy and geochemistry of shergottite RBT 04262. 39th Lunar and Planetary Science Conference, p. 2173. Lunar and Planetary Institute, League City, Texas.

Arcone, S.A., Prentice, M.L., and Delaney, A.J. (2002) Stratigraphic profiling with ground-penetrating radar in permafrost: A review of possible analogs for Mars. Journal of Geophysical Research: Planets, 107(E11).

Arvidson, R.E., Anderson, R., Bartlett, P., Bell, J., Blaney, D., Christensen, P., Chu, P., Crumpler, L., Davis, K., and Ehlmann, B. (2004) Localization and physical properties experiments conducted by Spirit at Gusev Crater. Science, 305(5685), 821-824.

Arvidson, R., Squyres, S., Anderson, R., Bell, J., Blaney, D., Brückner, J., Cabrol, N., Calvin, W., Carr, M., Christensen, P., and others (2006) Overview of the Spirit Mars Exploration rover mission to Gusev crater: Landing site to Backstay rock in the Columbia Hills. Journal of Geophysical Research: Planets (1991–2012), 111(E2).

Bandstra, J.Z., Buss, H.L., Campen, R.K., Liermann, L.J., Moore, J., Hausrath, E.M., Navarre-Sitchler, A.K., Jang, J.-H., and Brantley, S.L. (2008) Compilation of Mineral Dissolution Rates. In S. Brantley, J. Kubicki, and A. White, Eds. Kinetics of Water-Rock Interaction, p. 737-823. Springer, New York.

Barrat, J., Gillet, P., Sautter, V., Jambon, A., Javoy, M., Göpel, C., Lesourd, M., Keller, F., and Petit, E. (2002) Petrology and chemistry of the basaltic shergottite North West Africa 480. Meteoritics & Planetary Science, 37(4), 487-499.

Basu Sarbadhikari, A., Day, J.M., Liu, Y., Rumble, D., and Taylor, L.A. (2009) Petrogenesis of olivine-phyric shergottite Larkman Nunatak 06319: Implications for enriched components in Martian basalts. Geochimica et Cosmochimica Acta, 73(7), 2190-2214.

Berger, J.A., Schmidt, M.E., Gellert, R., Campbell, J.L., King, P.L., Flemming, R.L., Ming, D.W., Clark, B.C., Pradler, I., and VanBommel, S.J. (2016) A global Mars dust composition refined by the Alpha-Particle X-ray Spectrometer in Gale Crater. Geophysical Research Letters, 43(1), 67-75.

Bierman, P.R. (1994) Using in situ produced cosmogenic isotopes to estimate rates of landscape evolution: A review from the geomorphic perspective. Journal of Geophysical Research: Solid Earth, 99(B7), 13885-13896.

Bindeman, I.N., and Lowenstern, J.B. (2016) Low-δD hydration rinds in Yellowstone perlites record rapid syneruptive hydration during glacial and interglacial conditions. Contributions to Mineralogy and Petrology, 171(11), 89.

Bish, D.L., Blake, D., Vaniman, D., Chipera, S., Morris, R., Ming, D., Treiman, A., Sarrazin, P., Morrison, S., and Downs, R. (2013) X-ray diffraction results from Mars Science Laboratory: Mineralogy of Rocknest at Gale crater. Science, 341(6153), 1238932.

Blake, D.F., Morris, R., Kocurek, G., Morrison, S., Downs, R., Bish, D., Ming, D., Edgett, K., Rubin, D., and Goetz, W. (2013) Curiosity at Gale crater, Mars: Characterization and analysis of the Rocknest sand shadow. Science, 341(6153), 1239505.

Bogard, D.D., and Johnson, P. (1983) Martian gases in an Antarctic meteorite? Science, 221(4611), 651-654.

Brady, S., Hughes, S., Sakimoto, S., and Gregg, T. (2005) Exploring the link between geochemistry and volcano morphology on the Eastern Snake River Plain, a planetary analog to Mars volcanism. 36th Annual Lunar and Planetary Science Conference, Lunar and Planetary Institute, The Woodlands, Texas.

Brantley, S.L., and White, A.F. (2009) Approaches to modeling weathered regolith. Reviews in Mineralogy and Geochemistry, 70(1), 435-484.

Breed, C.S. (1977) Terrestrial analogs of the Hellespontus dunes, Mars. Icarus, 30(2), 326-340.

Brückner, J., Dreibus, G., Gellert, R., Squyres, S.W., Wänke, H., Yen, A., and Zipfel, J. (2008) Mars Exploration Rovers: chemical composition by the APXS. In J. Bell, Ed. The Martian Surface - Composition, Mineralogy, and Physical Properties, p. 58-100. Cambridge University Press, Cambridge.

Cavanagh, P., Bish, D., Blake, D., Vaniman, D., Morris, R., Ming, D., Rampe, E., Achilles, C., Chipera, S., and Treiman, A. (2015) Confidence Hills mineralogy and CheMin results from base of Mt. Sharp, Pahrump Hills, Gale Crater, Mars. [abstract 2735]. 46th Lunar and Planetary Science Conference, Lunar and Planetary Institute, Houston, Texas.

Christensen, P., Wyatt, M., Glotch, T., Rogers, A., Anwar, S., Arvidson, R., Bandfield, J., Blaney, D., Budney, C., and Calvin, W. (2004) Mineralogy at Meridiani Planum from the Mini-TES experiment on the Opportunity Rover. Science, 306(5702), 1733-1739.

Colman, S.M., and Pierce, K.L. (1981) Weathering rinds on andesitic and basaltic stones as a Quaternary age indicator, western United States. Geological Survey professional paper 1210, p. 41. United States Government Printing Office, Washington, D.C.

Crumpler, L.S., Arvidson, R.E., Squyres, S.W., McCoy, T., Yingst, A., Ruff, S., Farrand, W., McSween, Y., Powell, M., and Ming, D.W. (2011) Field reconnaissance geologic mapping of the Columbia Hills, Mars, based on Mars Exploration Rover Spirit and MRO HiRISE observations. Journal of Geophysical Research: Planets, 116(E7).

Curtiss, B., Adams, J.B., and Ghiorso, M.S. (1985) Origin, development and chemistry of silica-alumina rock coatings from the semi-arid regions of the island of Hawaii. Geochimica et Cosmochimica Acta, 49(1), 49-56.

Day, J., Taylor, L.A., Floss, C., and McSween, H.Y. (2006) Petrology and chemistry of MIL 03346 and its significance in understanding the petrogenesis of nakhlites on Mars. Meteoritics & Planetary Science, 41(4), 581-606.

Dehouck, E., McLennan, S.M., Meslin, P.Y., and Cousin, A. (2014) Constraints on abundance, composition, and nature of X-ray amorphous components of soils and rocks at Gale crater, Mars. Journal of Geophysical Research: Planets, 119(12), 2640-2657.

Dixon, E.M., Elwood Madden, A.S., Hausrath, E.M., and Elwood Madden, M.E. (2015) Assessing hydrodynamic effects on jarosite dissolution rates, reaction products, and preservation on Mars. Journal of Geophysical Research: Planets, 120(4), 625-642.

Dixon, J.C., Thorn, C.E., Darmody, R.G., and Campbell, S.W. (2002) Weathering rinds and rock coatings from an Arctic alpine environment, northern Scandinavia. Geological Society of America Bulletin, 114(2), 226-238.

Dreibus, G., Spettel, B., Haubold, R., Jochum, K., Palme, H., Wolf, D., and Zipfel, J. (2000) Chemistry of a new shergottite: Sayh al Uhaymir 005. Meteoritics and Planetary Science Supplement, 35, A49.

Farr, T.G., and Adams, J.B. (1984) Rock coatings in Hawaii. Geological Society of America Bulletin, 95(9), 1077-1083.

Fleischer, I., Klingelhöfer, G., Schröder, C., and Rodionov, D.S. (2008) Coatings and weathering rinds at Gusev crater, Mars, investigated by depth selective Mössbauer spectroscopy. Hyperfine Interactions, 186(1-3), 193-198.

Freeze, R.A., and Cherry, J.A. (1977) Groundwater. Prentice-Hall, New Jersey.

Gellert, R., Rieder, R., Anderson, R.C., Bruckner, J., Clark, B.C., Dreibus, G., Economou, T., Klingelhöfer, G., Lugmair, G.W., Ming, D.W., Squyres, S.W., d'Uston, C., Wanke, H., Yen, A., and Zipfel, J. (2004) Chemistry of Rocks and Soils in Gusev Crater from the Alpha Particle X-ray Spectrometer. Science, 305(5685), 829-832.

Gillet, P., Barrat, J., Beck, P., Marty, B., Greenwood, R., Franchi, I., Bohn, M., and Cotten, J. (2005) Petrology, geochemistry, and cosmic-ray exposure age of Iherzolitic shergottite Northwest Africa 1950. Meteoritics & Planetary Science, 40(8), 1175-1184.

Gislason, S.R., and Oelkers, E.H. (2003) Mechanism, rates and consequences of basaltic glass dissolution: II An experimental study of the dissolution rates of basaltic glass as a function of pH and temperature. Geochimica et Cosmochimica Acta, 67(20), 3817-3832.

Goldich, S. (1938) A study of rock weathering. Journal of Geology, 46, 17-58.

Goldstein, J.I., Newbury, D.E., Michael, J.R., Ritchie, N.W., Scott, J.H.J., and Joy, D.C. (2017) Scanning electron microscopy and X-ray microanalysis. Springer.

Golombek, M., Cook, R., Economou, T., Folkner, W., Haldemann, A., Kallemeyn, P., Knudsen, J.M., Manning, R., Moore, H., and Parker, T. (1997) Overview of the Mars Pathfinder mission and assessment of landing site predictions. Science, 278(5344), 1743-1748.

Gooding, J.L. (1992) Soil mineralogy and chemistry on Mars: Possible clues from salts and clays in SNC meteorites. Icarus, 99(1), 28-41.

Gordon, S.J., and Brady, P.V. (2002) In situ determination of long-term basaltic glass dissolution in the unsaturated zone. Chemical Geology, 190(1), 113-122.

Gorevan, S., Myrick, T., Davis, K., Chau, J., Bartlett, P., Mukherjee, S., Anderson, R., Squyres, S., Arvidson, R., and Madsen, M. (2003) Rock abrasion tool: Mars exploration rover mission. Journal of Geophysical Research: Planets, 108(E12).

Greeley, R., and King, J.S. (1977) Volcanism of the Eastern Snake River Plain, Idaho: A comparative planetary geology-guidebook. Arizona State University, Tempe

Greeley, R., Marshall, J., White, B., Pollack, J., Marshall, J., and Krinsley, D. (1984) Abrasion by aeolian particles: Earth and Mars. 303 p. NASA, Langley.

Greeley, R., and Iversen, J.D. (1987) Wind as a geological process: on Earth, Mars, Venus and Titan. Cambridge University Press, UK.

Greeley, R., and Fagents, S.A. (2001) Icelandic pseudocraters as analogs to some volcanic cones on Mars. Journal of Geophysical Research: Planets, 106(E9), 20527-20546.

Greeley, R., Bridges, N.T., Kuzmin, R.O., and Laity, J.E. (2002) Terrestrial analogs to wind-related features at the Viking and Pathfinder landing sites on Mars. Journal of Geophysical Research: Planets, 107(E1).

Grotzinger, J.P., Crisp, J., Vasavada, A.R., Anderson, R.C., Baker, C.J., Barry, R., Blake, D.F., Conrad, P., Edgett, K.S., and Ferdowski, B. (2012) Mars Science Laboratory mission and science investigation. Space Science Reviews, 170(1-4), 5-56.

Hamilton, V.E., and Ruff, S.W. (2012) Distribution and characteristics of Adirondack-class basalt as observed by Mini-TES in Gusev crater, Mars and its possible volcanic source. Icarus, 218(2), 917-949.

Haskin, L.A., Wang, A., Jolliff, B.L., McSween, H.Y., Clark, B.C., Des Marais, D.J., McLennan, S.M., Tosca, N.J., Hurowitz, J.A., and Farmer, J.D. (2005) Water alteration of rocks and soils on Mars at the Spirit rover site in Gusev crater. Nature, 436(7047), 66-69.

Hausrath, E.M., and Tschauner, O. (2013) Natural Fumarolic Alteration of Fluorapatite, Olivine, and Basaltic Glass, and Implications for Habitable Environments on Mars. Astrobiology, 13(11), 1049-1064.
Hausrath, E.M., Golden, D., Morris, R., and Ming, D. (2008a) Phosphate alteration on Mars. Geochimica et Cosmochimica Acta Supplement, 72, 357.
Hausrath, E.M., Navarre-Sitchler, A.K., Sak, P.B., Steefel, C.I., and Brantley, S.L. (2008b) Basalt weathering rates on Earth and the duration of liquid water on the plains of Gusev Crater, Mars. Geology, 36(1), 67-70.
Hausrath, E.M., Treiman, A.H., Vicenzi, E., Bish, D.L., Blake, D., Sarrazin, P., Hoehler, T., Midtkandal, I., Steele, A., and Brantley, S.L. (2008c) Short- and Long-Term Olivine Weathering in Svalbard: Implications for Mars. Astrobiology, 8(6), 1079-1092.
Heggy, E., Clifford, S.M., Grimm, R.E., Dinwiddie, C.L., Wyrick, D.Y., and Hill, B.E. (2006) Ground-penetrating radar sounding in mafic lava flows: Assessing attenuation and scattering losses in Mars-analog volcanic terrains. Journal of Geophysical Research: Planets, 111(E6).
Herkenhoff, K., Golombek, M., Guinness, E., Johnson, J., Kusack, A., Richter, L., Sullivan, R., and Gorevan, S. (2008) In situ observations of the physical properties of the martian surface. In I. Jim Bell, Ed. The Martian Surface-Composition, Mineralogy, and Physical Properties, p. 451. Cambridge University Press, New York.
Hess, S., Henry, R., Leovy, C., Ryan, J., Tillman, J., Chamberlain, T., Cole, H., Dutton, R., Greene, G., and Simon, W. (1976) Preliminary meteorological results on Mars from the Viking 1 lander. Science, 193(4255), 788-791.
Hurowitz, J.A., McLennan, S., Tosca, N., Arvidson, R., Michalski, J.R., Ming, D.W., Schroder, C., and Squyres, S.W. (2006a) In situ and experimental evidence for acidic weathering of rocks and soils on Mars. Journal of Geophysical Research, 111.
Hurowitz, J.A., and McLennan, S.M. (2007) A∼ 3.5 Ga record of water-limited, acidic weathering conditions on Mars. Earth and Planetary Science Letters, 260(3), 432-443.
Hurowitz, J.A., McLennan, S.M., McSween, H.Y., DeSouza, P.A.J., and Klingelhöfer, G. (2006b) Mixing relationships and the effects of secondary alteration in the Wishstone and Watchtower Classes of Husband Hill, Gusev Crater, Mars,. Journal of Geophysical Research, 111(E12S14), doi:10.1029/2006JE002795.
Ikeda, Y., Kimura, M., Takeda, H., Shimoda, G., Noriko, K., Morishita, Y., Suzuki, A., Jagoutz, E., and Dreibus, G. (2006) Petrology of a new basaltic shergottite: Dhofar 378. Antarctic Meteorite Research, 19, 20-44.
Jambon, A., Barrat, J., Sautter, V., Gillet, P., Göpel, C., Javoy, M., Joron, J., and Lesourd, M. (2002) The basaltic shergottite Northwest Africa 856: Petrology and chemistry. Meteoritics & Planetary Science, 37(9), 1147-1164.
Jin, L., Ravella, R., Ketchum, B., Bierman, P.R., Heaney, P., White, T., and Brantley, S.L. (2010) Mineral weathering and elemental transport during hillslope evolution at the Susquehanna/Shale Hills Critical Zone Observatory. Geochimica et Cosmochimica Acta, 74(13), 3669-3691.
Klingelhöfer, G. (2004) Mössbauer In Situ Studies of the Surface of Mars. Hyperfine Interactions, 158(1), 117-124.
Klingelhöfer, G., Morris, R., Bernhardt, B., Schröder, C., Rodionov, D., De Souza, P., Yen, A., Gellert, R., Evlanov, E., and Zubkov, B. (2004) Jarosite and hematite at Meridiani Planum from Opportunity's Mössbauer spectrometer. Science, 306(5702), 1740-1745.

DOI: http://dx.doi.org/10.2138/am-2018-6193

Kukachka, F.R. (2010) Soil survey of Craters of the Moon National Monument and Preserve, Idaho. United States Department of Agriculture, Natural Resources Conservation Service, and United States Department of the Interior, National Park Service., Washington D.C.

Kuntz, M.A., Covington, H.R., and Schorr, L.J. (1992) An overview of basaltic volcanism of the eastern Snake River Plain, Idaho. In P.K. Link, M.A. Kuntz, and L.B. Platt, Eds. Regional Geology of Eastern Idaho and Western Wyoming: Geological Society of America Memoir, 179, p. 227-266. Geological Society of America.

Kuntz, M.A., Elsheimer, N.H., Espos, L.F., and Klock, P.R. (1985) Major-element analyses of latest Pleistocene-Holocene lava fields of the Snake River Plain, Idaho. U.S. Dept. of the Interior, Geological Survey, Denver, CO.

Kuntz, M.A., Champion, D.E., Spiker, E.C., Lefebvre, R., and McBroome, L.A. (1982) The Great Rift and the evolution of the Craters of the Moon lava field, Idaho. Cenozoic Geology of Idaho: Idaho Bureau of Mines and Geology Bulletin, 26, 423-437.

Kuntz, M.A., Champion, D.E., Spiker, E.C., and Lefebvre, R.H. (1986a) Contrasting magma types and steady-state, volume-predictable, basaltic volcanism along the Great Rift, Idaho. Geological Society of America Bulletin, 97(5), 579-594.

Kuntz, M.A., Spiker, E.C., Rubin, M., Champion, D.E., and Lefebvre, R.H. (1986b) Radiocarbon studies of latest Pleistocene and Holocene lava flows of the Snake River Plain, Idaho: Data, lessons, interpretations. Quaternary Research, 25(2), 163-176.

Landvik, J.Y., Bondevik, S., Elverhoi, A., Fjeldskaar, W., Mangerud, J., Salvigsen, O., Siegert, M.J., Svendsen, J.-I., and Vorren, T.O. (1998) The last glacial maximum of Svalbard and the Barents sea area: ice sheet extent and configuration. Quaternary Science Reviews, 17(1-3), 43-75.

Leeman, W.P., Vitaliano, C.J., and Prinz, M. (1976) Evolved lavas from the snake river plain: craters of the moon national monument, Idaho. Contributions to Mineralogy and Petrology, 56(1), 35-60.

Levinthal, E., Green, W., Cutts, J., Jahelka, E., Johansen, R., Sander, M., Seidman, J., Young, A., and Soderblom, L. (1973) Mariner 9—Image processing and products. Icarus, 18(1), 75-101.

Lin, Y., Qi, L., Wang, G., and Xu, L. (2008) Bulk chemical composition of lherzolitic shergottite Grove Mountains 99027--Constraints on the mantle of Mars. Meteoritics & Planetary Science, 43(7), 1179.

Lodders, K. (1998) A survey of shergottite, nakhlite and chassigny meteorites whole-rock compositions. Meteoritics & Planetary Science, 33(S4), A183-A190.

McHenry, L.J. (2008) Unusual Sulfate Cave Mineral Deposits at Craters of the Moon National Monument, Idaho: Potential Analogue for Meridiani Planum, Mars. Wisconsin Space Conference, p. 10, Fitchberg.

McSween, H.Y. (2015) Petrology on Mars. American Mineralogist, 100(11-12), 2380-2395.

McSween, H.Y., Jr., Taylor, G.J., and Wyatt, M.B. (2009) Elemental Composition of the Martian Crust. Science, 324(5928), 736-739.

McSween, H.Y., Ruff, S., Morris, R., Bell, J., Herkenhoff, K., Gellert, R., Stockstill, K., Tornabene, L., Squyres, S., and Crisp, J. (2006) Alkaline volcanic rocks from the Columbia Hills, Gusev crater, Mars. Journal of Geophysical Research: Planets (1991–2012), 111(E9).

McSween, H.Y., Ruff, S.W., Morris, R.V., Gellert, R., Klingelhofer, G., Christensen, P.R., McCoy, T.J., Ghosh, A., Moersch, J.M., Cohen, B.A., Rogers, A.D., Schroder, C., Squyres, S.W., Crisp, J., and Yen, A. (2008) Mineralogy of volcanic rocks in Gusev Crater, Mars: Reconciling Mossbauer, Alpha Particle X-Ray Spectrometer, and Miniature Thermal Emission Spectrometer spectra. Journal of Geophysical Research, 113.

Millot, R., Gaillardet, J., Dupre, B., and Allegre, C.J. (2002) The global control of silicate weathering rates and the coupling with physical erosion: new insights from rivers of the Canadian Shield. Earth and Planetary Science Letters, 196(1-2), 83-93.

Ming, D.W., Mittlefehldt, D.W., Morris, R.V., Golden, D.C., Gellert, R., Yen, A., Clark, B.C., Squyres, S.W., Farrand, W.H., Ruff, S.W., Arvidson, R.E., Klingelho¨fer, G., McSween, H.Y., Rodionov, D.S., Schro¨ der, C., de Souza Jr., P.A., and Wang, A. (2006) Geochemical and mineralogical indicators for aqueous processes in the Columbia Hills of Gusev crater, Mars. Journal of Geophysical Research, 111(E02S12), doi:10.1029/2005JE002560.

Ming, D.W., Gellert, R., Morris, R.V., Arvidson, R.E., Brückner, J., Clark, B.C., Cohen, B.A., d'Uston, C., Economou, T., Fleischer, I., and others (2008) Geochemical properties of rocks and soils in Gusev Crater, Mars: Results of the Alpha Particle X-Ray Spectrometer from Cumberland Ridge to Home Plate. Journal of Geophysical Research, 113(E12), E12S39.

Myrick, T., Carlson, L., Chau, C., Powderly, J., Bartlett, P., Davis, K., and Gorevan, S. (2004) The RAT as a Mars Rock Physical Properties Tool. Space 2004 Conference and Exhibit, p. 6096. American Institute of Aeronautics and Astronautics, San Diego, California.

Navarre-Sitchler, A., and Brantley, S. (2007) Basalt weathering across scales. Earth and Planetary Science Letters, 261(1), 321-334.

Nishiizumi, K., Lal, D., Klein, J., Middleton, R., and Arnold, J. (1986) Production of 10Be and 26Al by cosmic rays in terrestrial quartz in situ and implications for erosion rates. Nature, 319(6049), 134-136.

Nishiizumi, K., Kohl, C., Arnold, J., Klein, J., Fink, D., and Middleton, R. (1991) Cosmic ray produced 10Be and 26Al in Antarctic rocks: exposure and erosion history. Earth and Planetary Science Letters, 104(2-4), 440-454.

Ody, A., Poulet, F., Quantin, C., Bibring, J.-P., Bishop, J., and Dyar, M. (2015) Candidates source regions of martian meteorites as identified by OMEGA/MEx. Icarus, 258, 366-383.

Oguchi, C.T., and Matsukura, Y. (1999) Effect of porosity on the increase in weathering-rind thicknesses of basaltic andesite gravel. Engineering Geology, 55(1-2), 77-89.

Olsen, A.A., Hausrath, E.M., and Rimstidt, J.D. (2015) Forsterite dissolution rates in Mg-sulfate-rich Mars-analog brines and implications of the aqueous history of Mars. Journal of Geophysical Research: Planets, 120(3), 388-400.

Owen, D.E. (2008) Geology of Craters of the Moon. 23 p. National Park Service, Washington D.C.

Palandri, J.L., and Kharaka, Y.K. (2004) A compilation of rate parameters of water-mineral interaction kinetics for application to geochemical modeling, p. 70. US Geological Survey, Menlo Park, CA.

Peck, S. (1974) Unusual Mineralogy of the Crystal Pit Spatter Cone, Craters of the Moon National Monument, Idaho. Bulletin National Speleological Society, 36(1), 19-24.

Phillips-Lander, C., Miller, K., Hausrath, E., Stockton, A., McCollum, N., and Elwood Madden, M. (2017) Light, Temperature, and Nutrient Availability Influence Microbial

Colonization of Lava Caves. 48th Lunar and Planetary Science Conference, p. 1964, Lunar and Planetary Institute, The Woodlands, Texas.

Porter, S.C. (1975) Weathering rinds as a relative-age criterion: application to subdivision of glacial deposits in the Cascade Range. Geology, 3(3), 101-104.

Pritchett, B., Madden, M.E., and Madden, A. (2012) Jarosite dissolution rates and maximum lifetimes in high salinity brines: Implications for Earth and Mars. Earth and Planetary Science Letters, 357, 327-336.

Putirka, K.D., Kuntz, M.A., Unruh, D.M., and Vaid, N. (2009) Magma evolution and ascent at the craters of the moon and neighboring volcanic fields, Southern Idaho, USA: implications for the evolution of polygenetic and monogenetic volcanic fields. Journal of Petrology, 50(9), 1639-1665.

Reid, M.R. (1995) Processes of mantle enrichment and magmatic differentiation in the eastern Snake River Plain: Th isotope evidence. Earth and Planetary Science Letters, 131(3), 239-254.

Rejeki, S., Hadi, J., and Suhayati, I. (2005) Porosity Study for Detail Reservoir Characterization in Darajat Geothermal Field, West Java, Indonesia. Proceedings of the World Geothermal Congress, Antalya, Turkey.

Richardson, C.D., Hinman, N.W., McHenry, L.J., Kotler, J.M., Knipe, D.L., and Scott, J.R. (2012) Secondary sulfate mineralization and basaltic chemistry of craters of the Moon National Monument, Idaho: Potential martian analog. Planetary and Space Science, 65(1), 93-103.

Richardson, C.D., Hinman, N.W., and Scott, J.R. (2013) Evidence for biological activity in mineralization of secondary sulphate deposits in a basaltic environment: implications for the search for life in the Martian subsurface. International Journal of Astrobiology, 12(4), 357-368.

Rieder, R., Gellert, R., Brückner, J., Klingelhöfer, G., Dreibus, G., Yen, A., and Squyres, S. (2003) The new Athena alpha particle X-ray spectrometer for the Mars Exploration Rovers. Journal of Geophysical Research: Planets, 108(E12).

Rubin, A.E. (1992) A shock-metamorphic model for silicate darkening and compositionally variable plagioclase in CK and ordinary chondrites. Geochimica et Cosmochimica Acta, 56(4), 1705-1714.

Rubin, A.E., Warren, P.H., Greenwood, J.P., Verish, R.S., Leshin, L.A., Hervig, R.L., Clayton, R.N., and Mayeda, T.K. (2000) Los Angeles: The most differentiated basaltic martian meteorite. Geology, 28(11), 1011-1014.

Ruff, S.W., Christensen, P.R., Blaney, D.L., Farrand, W.H., Johnson, J.R., Michalski, J.R., Moersch, J.E., Wright, S.P., and Squyres, S.W. (2006) The rocks of Gusev Crater as viewed by the Mini-TES instrument. Journal of Geophysical Research, 111(E12S18), doi:10.1029/2006JE002747.

Russell, I.C. (1903) Notes on the geology of southwestern Idaho and southeastern Oregon. US Government Printing Office, Washington D.C.

Sak, P.B., Fisher, D.M., Gardner, T.W., Murphy, K., and Brantley, S.L. (2004) Rates of weathering rind formation on Costa Rican basalt. Geochimica et Cosmochimica Acta, 68(7), 1453-1472.

Salvatore, M., Mustard, J., Head, J., Cooper, R., Marchant, D., and Wyatt, M. (2013) Development of alteration rinds by oxidative weathering processes in Beacon Valley, Antarctica, and implications for Mars. Geochimica et Cosmochimica Acta, 115, 137-161.

Santos, A.R., Agee, C.B., McCubbin, F.M., Shearer, C.K., Burger, P.V., Tartèse, R., and Anand, M. (2015) Petrology of igneous clasts in Northwest Africa 7034: Implications for the petrologic diversity of the Martian crust. Geochimica et Cosmochimica Acta, 157, 56-85.

Sato, H., Shibutani, T., and Yui, M. (1997) Experimental and modeling studies on diffusion of Cs, Ni and Sm in granodiorite, basalt and mudstone. Journal of Contaminant Hydrology, 26, 119-133.

Saunders, R., Arvidson, R., Badhwar, G., Boynton, W.V., Christensen, P., Cucinotta, F., Feldman, W., Gibbs, R., Kloss Jr, C., and Landano, M. (2004) 2001 Mars Odyssey mission summary. 2001 Mars Odyssey, p. 1-36. Springer.

Sautter, V., Toplis, M., Wiens, R., Cousin, A., Fabre, C., Gasnault, O., Maurice, S., Forni, O., Lasue, J., and Ollila, A. (2015) In situ evidence for continental crust on early Mars. Nature Geoscience, 8(8), 605-609.

Schieber, J., Bish, D., Coleman, M., Reed, M., Hausrath, E.M., Cosgrove, J., Gupta, S., Minitti, M.E., Edgett, K.S., and Malin, M. (2016) Encounters with an unearthly mudstone: Understanding the first mudstone found on Mars. Sedimentology, 64(2), 311-358.

Schroeder, C., Klingelhoefer, G., Morris, R., and Rodionov, D. (2006) Weathering of Rocks in Gusev Crater Inferred From Correlations Between Primary and Secondary Fe-bearing Minerals Identified by Spirit's Moessbauer Spectrometer. AGU Fall Meeting Abstracts, American Geophysical Union, San Fransico, California.

Sharp, R.P. (1964) Wind-driven sand in Coachella valley, California. Geological Society of America Bulletin, 75(9), 785-804.

Sharp, R.P. (1980) Wind-driven sand in Coachella Valley, California: further data. Geologic Society of America Bulletin, 91(12), 724-730.

Shirai, N., and Ebihara, M. (2004) Chemical characteristics of a Martian meteorite, Yamato 980459. Antarctic Meteorite Research, 17, 55.

Smith, P., Tamppari, L., Arvidson, R., Bass, D., Blaney, D., Boynton, W., Carswell, A., Catling, D., Clark, B., and Duck, T. (2008) Introduction to special section on the phoenix mission: landing site characterization experiments, mission overviews, and expected science. Journal of Geophysical Research: Planets, 113(E3).

Snyder, C.W., and Moroz, V.I. (1992) Spacecraft exploration of Mars. Mars, 1, 71-119. University of Arizona Press, Tucson.

Soderblom, L., and Bell III, J. (2008) Exploration of the Martian surface: 1992-2007. The Martian Surface-Composition, Mineralogy, and Physical Properties, 1, 3.

Squyres, S.W., Arvidson, R.E., Blaney, D.L., Clark, B.C., Crumpler, L., Farrand, W.H., Gorevan, S., Herkenhoff, K.E., Hurowitz, J., Kusack, A., McSween, H.Y., Ming, D.W., Morris, R.V., Ruff, S.W., Wang, A., and Yen, A. (2006) Rocks of the Columbia Hills. Journal of Geophysical Research: Planets, 111(E2), E02S11.

Stearns, H.T. (1924) Craters of the Moon National Monument. Geographical Review, 14(3), 362-372.

-. (1928) Craters of the Moon National Monument. In E. Ellis, Ed. Idaho Bureau of Mines and Geology Bulletin, 13, p. 57. Idaho Bureau of Mines and Geology, Moscow.

Steinbacher, R., Kliore, A., Lorell, J., Hipsher, H., Barth, C., Masursky, H., Münch, G., Pearl, J., and Smith, B. (1972) Mariner 9 science experiments-Preliminary results. Science, 175(4019), 293-294.

Steiner, M., Hausrath, E., Madden, M.E., Tschauner, O., Ehlmann, B., Olsen, A., Gainey, S., and Smith, J. (2016) Dissolution of nontronite in chloride brines and implications for the aqueous history of Mars. Geochimica et Cosmochimica Acta, 195, 259-276.

Stöffler, D., Ostertag, R., Jammes, C., Pfannschmidt, G., Gupta, P.S., Simon, S., Papike, J., and Beauchamp, R. (1986) Shock metamorphism and petrography of the Shergotty achondrite. Geochimica et Cosmochimica Acta, 50(6), 889-903.

Stout, M.Z., Nicholls, J., and Kuntz, M.A. (1994) Petrological and mineralogical variations in 2500-2000 yr B.P. lava flows, Craters of the Moon lava field, Idaho. Journal of Petrology, 35(6), 1681-1681-1715.

Stuiver, M., and Reimer, P.J. (1993) Extended 14 C data base and revised CALIB 3.0 14 C age calibration program. Radiocarbon, 35(01), 215-230.

Taylor, G.J. (2013) The bulk composition of Mars. Chemie Der Erde-Geochemistry, 73(4), 401-420.

Thomson, B., Bridges, N., Cohen, J., Hurowitz, J., Lennon, A., Paulsen, G., and Zacny, K. (2013) Estimating rock compressive strength from Rock Abrasion Tool (RAT) grinds. Journal of Geophysical Research: Planets, 118(6), 1233-1244.

Treiman, A.H., and Irving, A.J. (2008) Petrology of martian meteorite Northwest Africa 998. Meteoritics & Planetary Science, 43(5), 829-854.

Udry, A., Lunning, N.G., McSween, H.Y., and Bodnar, R.J. (2014) Petrogenesis of a vitrophyre in the martian meteorite breccia NWA 7034. Geochimica et Cosmochimica Acta, 141, 281-293.

Usui, T., McSween, H.Y., and Clark, B.C. (2008) Petrogenesis of high-phosphorous Wishstone Class rocks in Gusev Crater, Mars. Journal of Geophysical Research, 113(E12S44), doi:10.1029/2008JE003225.

Vaughan, K.L. (2008) Pedogenesis at Craters of the Moon National Monument and Preserver, Idaho, USA. Department of Soil Science, Ph.D., p. 156. University of Idaho, Moscow.

Vaughan, K.L., and McDaniel, P.A. (2009) Organic soils on basaltic lava flows in a cool, arid environment. Soil Science Society of America Journal, 73(5), 1510-1518.

Vaughan, K.L., McDaniel, P.A., and Phillips, W.M. (2011) Episodic soil succession on basaltic lava fields in a cool, dry environment. Soil Science Society of America Journal, 75(4), 1462-1470.

Walton, E.L., and Herd, C.D. (2007) Dynamic crystallization of shock melts in Allan Hills 77005: implications for melt pocket formation in Martian meteorites. Geochimica et Cosmochimica Acta, 71(21), 5267-5285.

Wang, A., Haskin, L.A., Squyres, S.W., Jolliff, B.L., Crumpler, L., Gellert, R., Schröder, C., Herkenhoff, K., Hurowitz, J., and Tosca, N.J. (2006a) Sulfate deposition in subsurface regolith in Gusev crater, Mars. Journal of Geophysical Research: Planets (1991–2012), 111(E2).

Wang, A., Korotev, R.L., Jolliff, B.L., Haskin, L.A., Crumpler, L., Farrand, W.H., Herkenhoff, K.E., de Souza, P., Kusack, A.G., and Hurowitz, J.A. (2006b) Evidence of phyllosilicates in Wooly Patch, an altered rock encountered at West Spur, Columbia Hills, by the Spirit rover in Gusev crater, Mars. Journal of Geophysical Research: Planets, 111(E2).

Wanke, H., and Dreibus, G. (1988) Chemical Composition and Accretion History of Terrestrial Planets. Philosophical Transactions of the Royal Society of London. Series A, Mathematical and Physical Sciences, 325(1587), 545-557.

Weren, S., Sakimoto, S., Hughes, S., and Gregg, T. (2004) Comparison of plains volcanism in the Tempe Terra region of Mars to the Eastern Snake River Plains, Idaho with implications for geochemical constraints. Lunar and Planetary Science Conference, 35, p. 2090.

Wheater, C.P., and Cook, P.A. (2006) Using statistics to understand the environment. 245 p., Routledge, New York.

Wierzchos, J., Ascaso, C., and McKay, C.P. (2006) Endolithic cyanobacteria in halite rocks from the hyperarid core of the Atacama Desert. Astrobiology, 6(3), 415-422.

Wolff-Boenisch, D., Gislason, S.R., Oelkers, E.H., and Putnis, C.V. (2004) The dissolution rates of natural glasses as a function of their composition at pH 4 and 10.6, and temperatures from 25 to 74[deg]C. Geochimica et Cosmochimica Acta, 68(23), 4843-4858.

Wynn-Williams, D., and Edwards, H. (2000) Proximal analysis of regolith habitats and protective biomolecules in situ by laser Raman spectroscopy: overview of terrestrial Antarctic habitats and Mars analogs. Icarus, 144(2), 486-503.

Yen, A., Blake, D., Ming, D., Morris, R., Gellert, R., Clark, B., Vaniman, D., Chipera, S., Thompson, L., and Bristow, T. (2016) Cementation and aqueous alteration of a sandstone unit under acidic conditions in Gale Crater, Mars. 47th Lunar and Planetary Science Conference, p. 1649. Lunar and Planetary Institute, The Woodlands, Texas.

Yesavage, T., Thompson, A., Hausrath, E.M., and Brantley, S.L. (2015) Basalt weathering in an Arctic Mars-analog site. Icarus, 254, 219-232.

Zipfel, J., Schroeder, C., Jolliff, B.L., Gellert, R., Herkenhoff, K.E., Rieder, R., Anderson, R., BELL III, J.F., Brueckner, J., and Crisp, J.A. (2011) Bounce Rock—A shergottite-like basalt encountered at Meridiani Planum, Mars. Meteoritics & Planetary Science, 46(1), 1-20.

Zurek, R.W., and Smrekar, S.E. (2007) An overview of the Mars Reconnaissance Orbiter (MRO) science mission. Journal of Geophysical Research: Planets, 112(E5).

FIGURE CAPTIONS

Figure 1. Craters of the Moon National Monument sampling locations and associated flow ages. Inset shows general location within the state of Idaho (red box). Enhanced USGS LANDSAT 8 color shortwave-infrared image, bands 7-4-3 displayed as R-G-B. Different dark colors in flow fields represent different individual flows. Ages determined by radio-carbon dating, y.b.p. = years before present.

Figure 2. **TAS (Na_2O + K_2O versus SiO_2) diagram of COTM basalts, martian meteorites, and martian surface compositions.** Plot shows most COTM rocks materials are generally higher in Na_2O+K_2O content compared to the martian materials. There are a few exceptions including some high-phosphorus rocks analyzed at Gusev Crater (Watchtower and Wishstone class), some of the clasts of NWA 7034, and alkali rocks analyzed at Gale Crater. Note trend in COTM basalts of increasing alkalis with increasing SiO_2. The relationship generally follows the age of COTM flows with lower SiO_2 and alkali contents typical of the older flows.

Figure 3. A) FeO total versus MgO, B) P_2O_5 versus MgO, C) CaO versus MgO, and D) Al_2O_3 versus MgO (all in wt.%). COTM rocks tend to be lower in MgO and higher in Al_2O_3 than the martian materials, although there are several exceptions (e.g. Wishstone class rocks). The linear trend seen in COTM rocks in some plots is a result of the evolution of volcanism at COTM over time. The higher MgO, CaO, and FeO contents are typical of the older flows at COTM.

Figure 4. BSE images of textures typical of the six flows sampled at exposed edges. A) Blue Dragon, B) Minidoka, C) Lava Point, D) Prong Horn, E) Sunset, and F) Kimama. Note differences

in matrix material with Blue Dragon and Minidoka being mainly glass and the other samples being more crystalline and less glassy. Coatings, like those of Lava Point (C) and Prong Horn (D) were found on all samples with exposed surfaces, but were not continuous on the surfaces. Plg = plagioclase, Ol = olivine, Mt = magnetite/ilmenite, Px = pyroxene, gls = glass, Ap = apatite. All scale bars 100 µm.

Figure 5. BSE image of Kimama basalt in thin section. Image shows development of porosity (A) below discontinuous surface coating (B). The porosity appears to be from the dissolution of glass in the groundmass. Phynocrysts show no obvious signs of dissolution. Pl = plagioclase, Olv = olivine, Mt = magnetite/ilmenite, Px = pyroxene, gls = glass. Scale bar = 50 µm.

Figure 6. BSE image of Blue Dragon basalt in thin section. Note dark layer (indicated with an arrow). The dark layer possessed very similar chemistry by EDS to the brighter glass material beneath it. This may indicate the dark material is hydrated. Pl = plagioclase, Ol = olivine, gls = glass, Ap = apatite. Scale bar is 50 µm.

Figure 7: Depth of developed porosity (µm) versus age plots (years b.p.) for the three approaches of interpretation. A) All methods combined. **B)** Quantitative method (Supplementary Figure S2). **C)** Judged visually from BSE image profile (Supplementary Figure S3). **D)** Judged visually from plotted profile (Supplementary Figure S1). Regression intercepts were tied to zero. No weighting given to associated errors for regression analysis. Note: all axes are identical.

TABLES

Table 1. ^{14}C ages of flows at Craters of the Moon National Monument

Flow	Eruptive Period	Reference	Age (y.b.p.)[a]	Error +/- (years)	Calibrated Age (y.b.p.)[a,b]
Kimama	H	1	15100	160	18340
Lava Creek	G	1	12760	150	15180
Sunset	G	1	12010	150	13870
Carey	G	1	12000	150	13860
Heifer Reservoir	F	1	10670	150	12580
Bottleneck Lake	F	1	11000	100	12890
Pronghorn	F	1	10240	120	11970
Lava Point	F	1	7840	140	8690
Laidlaw Lake	E	1	7470	80	8280
Grassy Cone	E	1	7360	60	8180
Little Park	D	1	6500	60	7410
Carey Kupuka	D	1	6600	60	7500
Silent Cone	D	2	6500	nr	7410
Sentinel	C	2	6000	nr	6840
Fissure Butte	C	2	6000	nr	6840
Sheep Trail	C	2	6000	nr	6840
Sawtooth	C	2	6000	nr	6880
Indian Wells N.	C	1	6020	160	6880
Rangefire	B	1	4510	100	5150
Minidoka	B	1	3590	70	3890
Devils Cauldron	B	1	3660	60	3990
Deadhourse	A	1	4300	60	4880
Highway	A	2	2400	nr	2460
Serrate	A	2	2400	nr	2460
Big Craters (Green Dragon)	A	1	2400	300	2450
Trench Mortar Flat	A	1	2180	70	2190
Blue Dragon	A	1	2076	45	2050

References: 1 = (Kuntz et al., 1986b) 2 = (Kuntz et al., 1992). [a]y.b.p. = years before present. [b]Ages calibrated using Calib 7.0.4 with InterCal 13 (Stuiver and Reimer, 1993).

Table 2. Average analyses (wt.%) of basalts by eruptive period at Craters of the Moon National Monument

	Eruptive Period									
	H	**G**	**F**	**E**	**D**	**C**	**C low**	**B**	**A**	**A low**
SiO_2	45.24	46.79	46.05	46.45	50.93	46.19	56.29	48.57	50.71	61.40
TiO_2	3.28	3.12	3.27	3.43	2.28	3.25	1.50	2.95	2.66	0.81
Al_2O_3	14.23	14.05	13.62	12.94	14.17	13.71	14.89	13.84	13.54	14.22
FeO	15.11	13.39	14.84	10.87	12.76	8.63	10.72	14.17	13.35	7.51
MnO	0.28	0.26	0.26	0.24	0.23	0.26	0.21	0.24	0.24	0.18
MgO	4.53	4.09	4.16	4.25	2.64	4.43	1.70	3.69	3.02	0.40
CaO	7.50	7.61	8.13	8.29	6.05	8.10	4.54	7.02	6.84	3.25
Na_2O	3.50	3.81	3.71	3.31	4.02	3.42	4.05	3.90	3.58	4.10
K_2O	1.75	1.96	1.88	1.74	2.46	1.77	3.22	1.98	2.24	4.28
P_2O_5	2.64	2.21	2.32	2.23	1.40	2.38	0.75	2.00	1.56	0.22
Total	98.06	100.19	99.83	99.30	98.63	100.20	99.50	99.88	99.26	98.39
n	1	3	2	2	2	3	2	2	4	2

n= number of flows average is based on. Based on analyses from Kuntz et al., (1992) and Kuntz et al., (1985)

DOI: http://dx.doi.org/10.2138/am-2018-6193

Table 3. Best matches between martian materials and rocks from COTM eruptive periods

	Martian Materials[1]	**Most Comparable COTM Eruptive Period[3]**
NWA 7034 Clasts	6[2]	Period H
	56	Period C low
	66	Period B
	70	Periods E, F, G, H
	74F	Period A
Gusev Crater	Champagne[2]	Period H
	Wishtone	Period E, G, H
	Watchtower	Period H
Gale Crater	Becraft[2]	Periods A low, C low
	Chakonipau	Period A low
	Sledgers	Period A low

[1] Best matches only. Complete lists of material considered in this study are in Appendix Tables A2 to A7.

[2] Produced best fit for group.

[3] Based on chemical composition and normative mineralogy

FIGURES

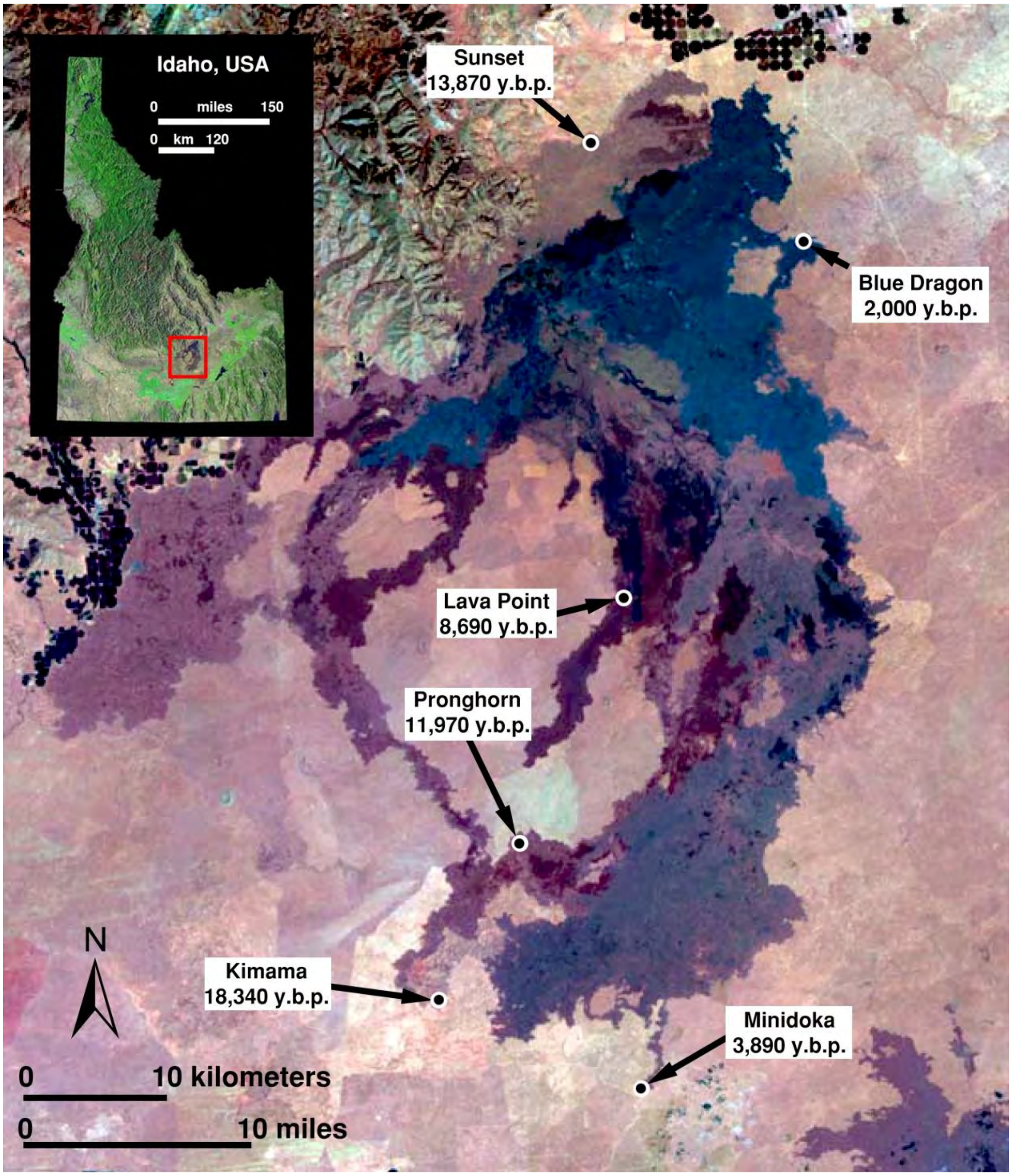

Figure 1. Craters of the Moon National Monument sampling locations and associated flow ages. Inset shows general location within the state of Idaho (red box). Enhanced USGS LANDSAT 8 color shortwave-infrared image, bands 7-4-3 displayed as R-G-B. Different dark colors in flow

fields represent different individual flows. Ages determined by radio-carbon dating, y.b.p. = years before present.

This is a preprint, the final version is subject to change, of the American Mineralogist (MSA)
Cite as Authors (Year) Title. American Mineralogist, in press.
DOI: http://dx.doi.org/10.2138/am-2018-6193

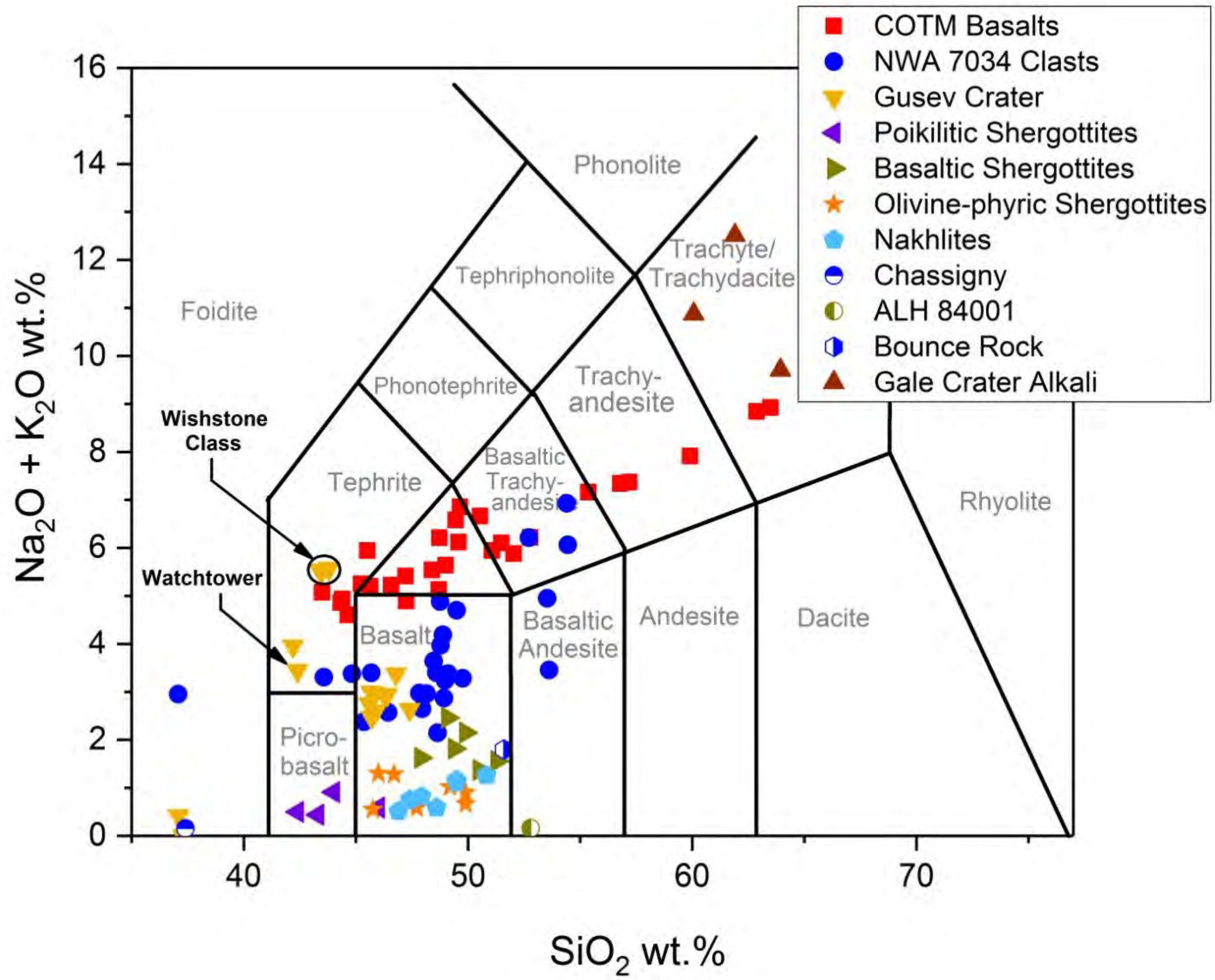

Figure 2. **TAS ($Na_2O + K_2O$ versus SiO_2) diagram of COTM basalts, martian meteorites, and martian surface compositions.** Plot shows most COTM rocks materials are generally higher in Na_2O+K_2O content compared to the martian materials. There are a few exceptions including some high-phosphorus rocks analyzed at Gusev Crater (Watchtower and Wishstone class), some of the clasts of NWA 7034, and alkali rocks analyzed at Gale Crater. Note trend in COTM basalts of increasing alkalis with increasing SiO_2. The relationship generally follows the age of COTM flows with lower SiO_2 and alkali contents typical of the older flows.

This is a preprint, the final version is subject to change, of the American Mineralogist (MSA)
Cite as Authors (Year) Title. American Mineralogist, in press.
DOI: http://dx.doi.org/10.2138/am-2018-6193

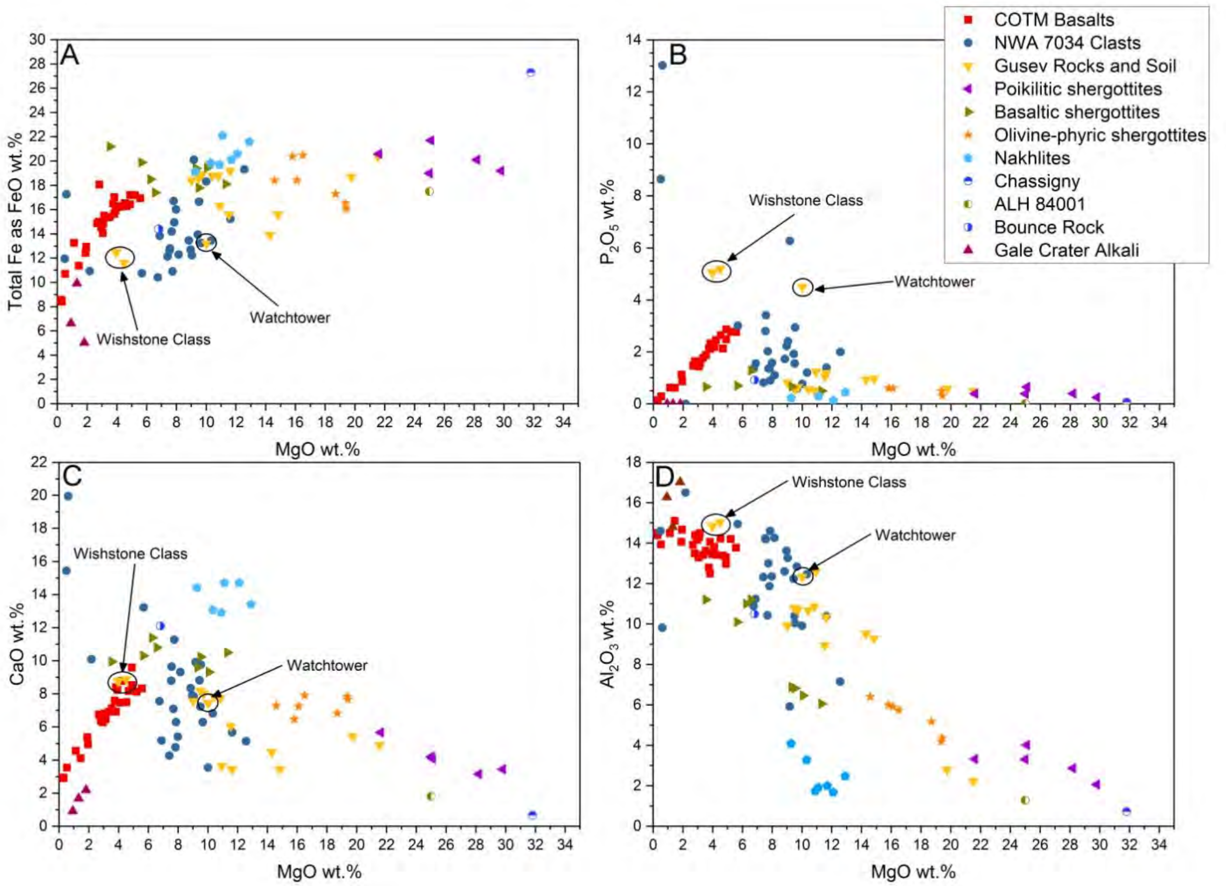

Figure 3. A) FeO total versus MgO, B) P_2O_5 versus MgO, C) CaO versus MgO, and D) Al_2O_3 versus MgO (all in wt.%). COTM rocks tend to be lower in MgO and higher in Al_2O_3 than the martian materials, although there are several exceptions (e.g. Wishstone class rocks). The linear trend seen in COTM rocks in some plots is a result of the evolution of volcanism at COTM over time. The higher MgO, CaO, and FeO contents are typical of the older flows at COTM.

DOI: http://dx.doi.org/10.2138/am-2018-6193

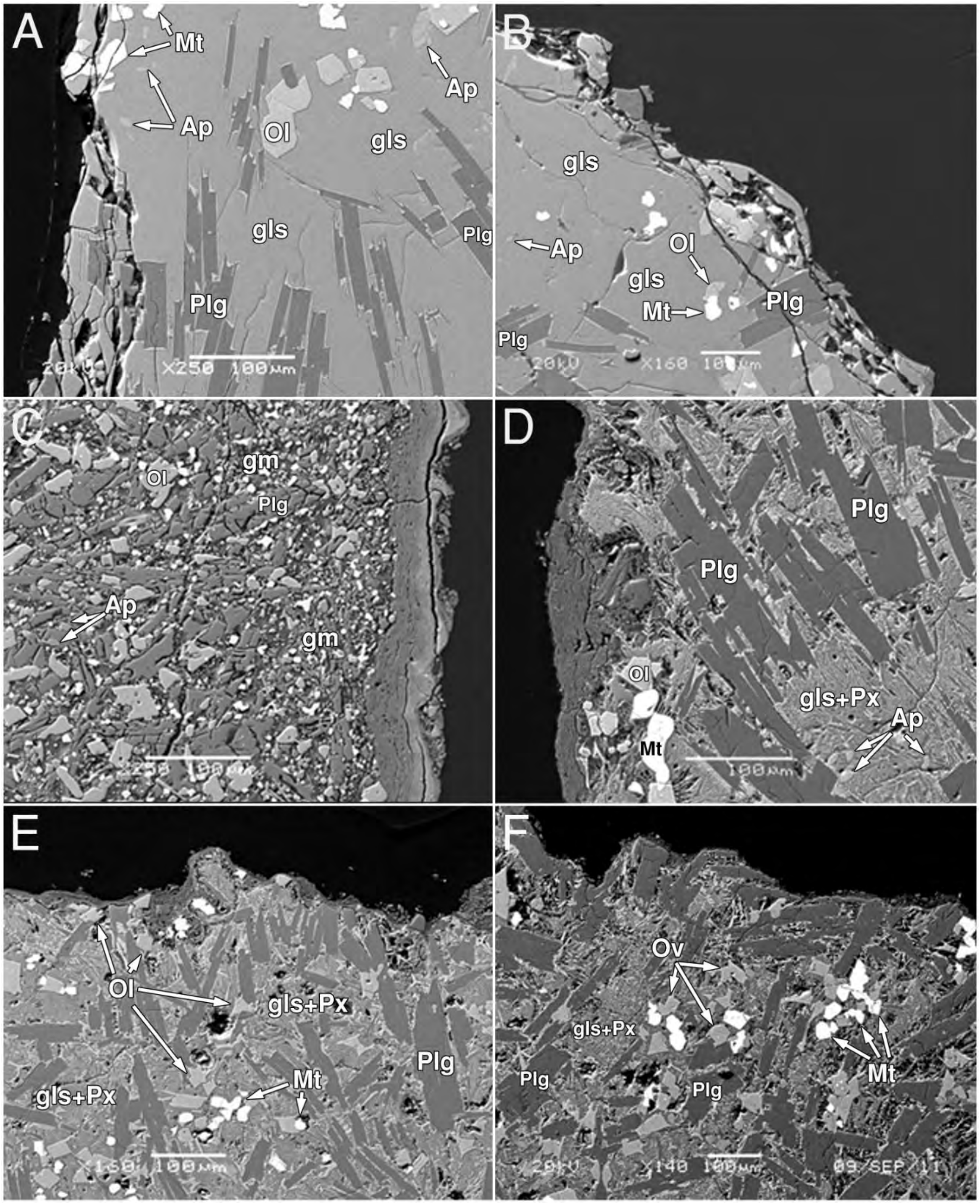

Figure 4. BSE images of textures typical of the six flows sampled at exposed edges. A) Blue Dragon, B) Minidoka, C) Lava Point, D) Prong Horn, E) Sunset, and F) Kimama. Note differences in matrix material with Blue Dragon and Minidoka being mainly glass and the other samples

being more crystalline and less glassy. Coatings, like those of Lava Point (C) and Prong Horn (D) were found on all samples with exposed surfaces, but were not continuous on the surfaces. Plg = plagioclase, Ol = olivine, Mt = magnetite/ilmenite, Px = pyroxene, gls = glass, Ap = apatite. All scale bars 100 µm.

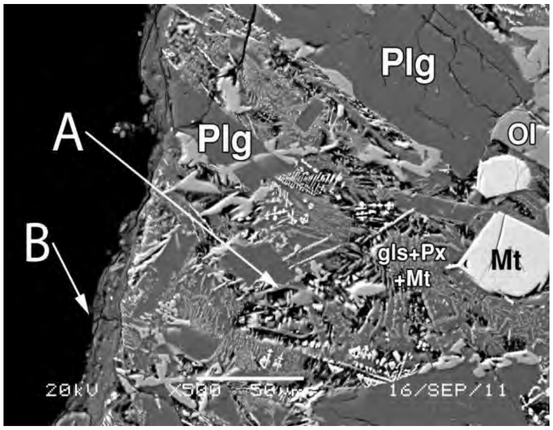

Figure 5. BSE image of Kimama basalt in thin section. Image shows development of porosity (A) below discontinuous surface coating (B). The porosity appears to be from the dissolution of glass in the groundmass. Phynocrysts show no obvious signs of dissolution. Pl = plagioclase, Olv = olivine, Mt = magnetite/ilmenite, Px = pyroxene, gls = glass. Scale bar = 50 µm.

DOI: http://dx.doi.org/10.2138/am-2018-6193

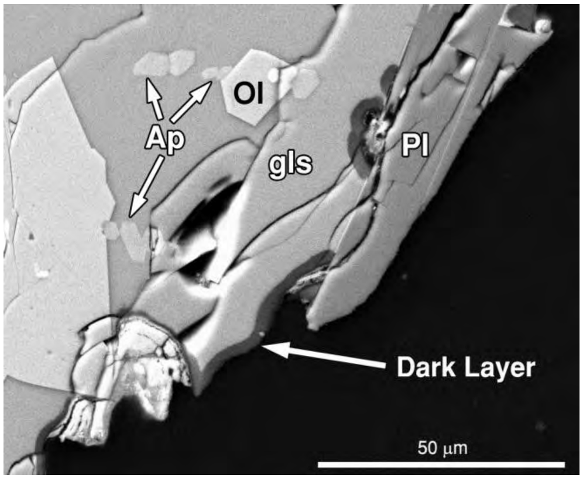

Figure 6. BSE image of Blue Dragon basalt in thin section. Note dark layer (indicated with an arrow). The dark layer possessed very similar chemistry by EDS to the brighter glass material beneath it. This may indicate the dark material is hydrated. Pl = plagioclase, Ol = olivine, gls = glass, Ap = apatite. Scale bar is 50 µm.

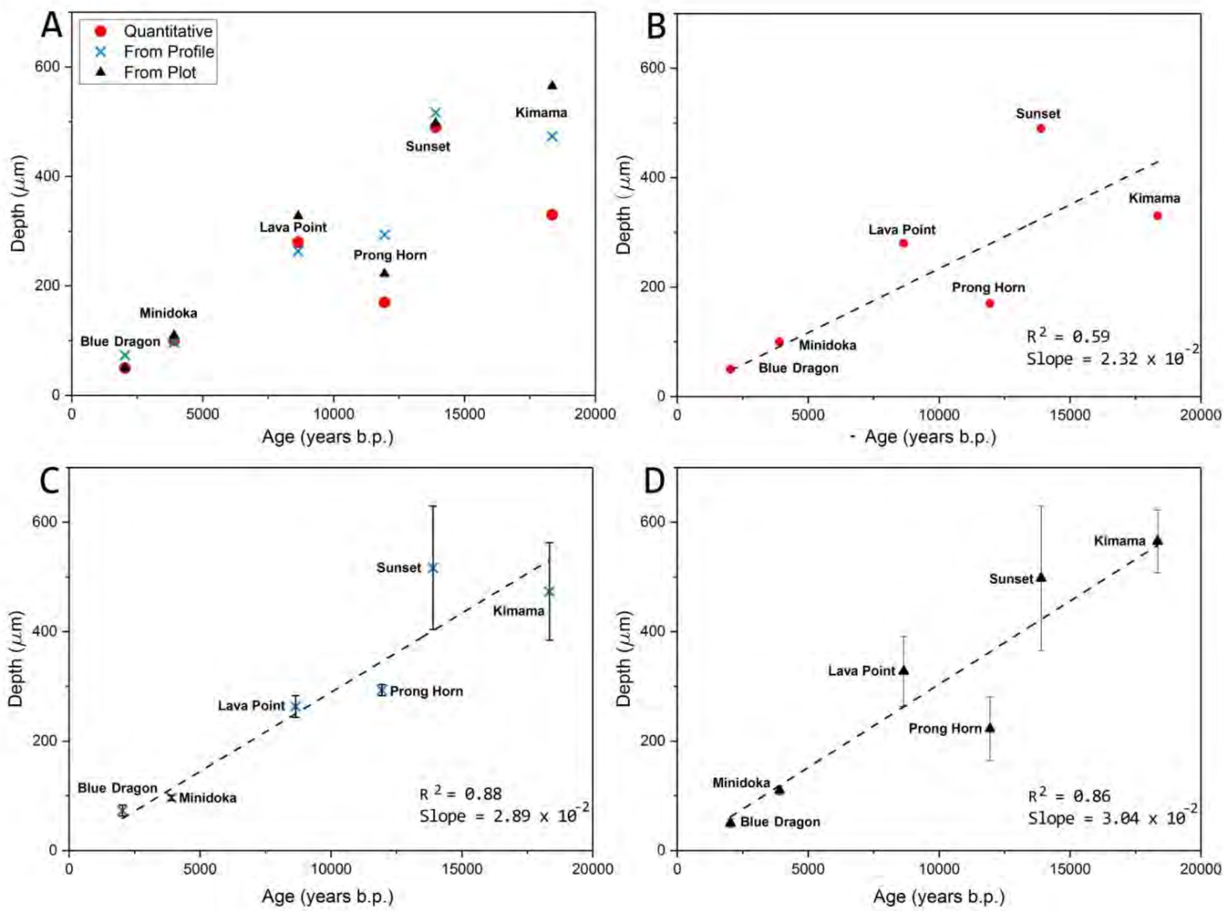

Figure 7: Depth of developed porosity (μm) versus age plots (years b.p.) for the three approaches of interpretation. A) All methods combined. **B)** Quantitative method (Supplementary Figure S2). **C)** Judged visually from BSE image profile (Supplementary Figure S3). **D)** Judged visually from plotted profile (Supplementary Figure S1). Regression intercepts were tied to zero. No weighting given to associated errors for regression analysis. Note: all axes are identical.